ANKARA UNIVERSITY
GRADUATE SCHOOL OF NATURAL AND APPLIED SCIENCES

MASTER THESIS

INVESTIGATING THE EFFECTS OF GRAPHENE OXIDE OF DIFFERENT SIZES ON IMMUNE CELLS IN STATIC AND DYNAMIC ENVIRONMENTS

Oğuzhan PANATLI

DEPARTMENT OF BIOMEDICAL ENGINEERING

ANKARA
2022

ABSTRACT

M.Sc. Thesis

INVESTIGATING THE EFFECTS OF GRAPHENE OXIDE OF DIFFERENT SIZES ON IMMUNE CELLS IN STATIC AND DYNAMIC ENVIRONMENTS

Oğuzhan PANATLI

Ankara University
Graduate School of Natural and Applied Sciences
Department of Biomedical Engineering

Supervisor: Assoc. Prof. Dr. Açelya YILMAZER AKTUNA

Graphene and its derivatives have significant properties. Studies are carried out on these nanomaterials in various fields such as biomedical, nanomedicine, and nanotechnology. Research on the biocompatibility of graphene oxide, which is one of the graphene-based materials, continues today. Although the conventional cell culture method is a very valuable method that are used in *in vitro* studies for many decades, it is insufficient to fully mimic the nuances of cellular microenvironment. Nowadays, three-dimensional cell culture and microfluidic cell culture are used in order to overcome this unfavorable situation. In this thesis, the biocompatibility of graphene oxide was investigated. To this end, the effect of graphene oxide that has two different sizes on Jurkat cells were addressed. In addition, the cellular response of these cells to graphene oxide in both static (conventional cell culture) and dynamic (microfluidic cell culture) environments was examined. In *in vitro* studies, the viability of Jurkat cells that treated with graphene oxide in different sizes was tested. The obtained data indicated that the cell viability changed depending on the size of graphene oxide and the cell culture environment. As a consequence, it is thought that examining the cell-nanomaterial interaction in static and dynamic cell cultures is important for understanding the biocompatibility of different sizes of graphene oxide.

August 2022, 67 Pages

Key Words: Conventional cell culture, microfluidic cell culture, graphene oxide, toxicity, nanomaterial

ÖZET

Yüksek Lisans Tezi

FARKLI BOYUTLARDAKİ GRAFEN OKSİTİN STATİK VE DİNAMİK ORTAMLARDAKİ BAĞIŞIKLIK HÜCRELERİ ÜZERİNE ETKİLERİNİN ARAŞTIRILMASI

Oğuzhan PANATLI

Ankara Üniversitesi
Fen Bilimleri Enstitüsü
Biyomedikal Mühendisliği Anabilim Dalı

Danışman: Doç. Dr. Açelya YILMAZER AKTUNA

Grafen ve türevleri önemli özelliklere sahiptir. Biyomedikal, nanotıp, nanoteknoloji gibi çeşitli alanlarda bu nanomalzemeler üzerine çalışmalar yapılmaktadır. Günümüzde grafen temelli nanomalzemelerden biri olan grafen oksitin biyouyumluluğu üzerine araştırmalar devam etmektedir. Geleneksel hücre kültürü, *in vitro* çalışmalarda yıllardır kullanılan çok değerli bir yöntem olmasına rağmen, hücresel ortamın nüanslarını özgün olarak yansıtmada yetersizdir. Bu durumun üstesinden gelmek amacıyla, 3 boyutlu hücre kültürü ve mikroakışkan hücre kültürü yöntemleri kullanılmaktadır. Bu tez kapsamında; grafen oksitin biyouyumluluğu araştırılmıştır. Bu amaçla, iki farklı boyuttaki grafen oksitin Jurkat hücreleri üzerindeki etkisi ele alınmıştır. Ayrıca, Jurkat hücrelerin hem statik (geleneksel hücre kültürü) hem de dinamik (mikroakışkan hücre kültürü) ortamlarda, grafen oksite verdiği hücresel yanıt incelenmiştir. *In vitro* tahlillerde, farklı boyutlarda grafen oksit ile muamele edilen Jurkat hücrelerinin canlılığı test edilmiştir. Mevcut veriler, hücre canlılığının grafen oksitin boyutuna ve hücre kültürü ortamına bağlı olarak değiştiğini göstermektedir. Sonuç olarak, statik ve dinamik hücre kültürlerindeki hücre-nanomalzeme etkileşiminin incelenmesinin farklı boyutlardaki grafen oksitin biyouyumluluğunu anlamada önemli olduğu düşünülmektedir.

Ağustos 2022, 67 Sayfa

Anahtar kelimeler: Geleneksel hücre kültürü, mikroakışkan hücre kültürü, grafen oksit, toksisite, nanomalzeme

ACKNOWLEDGEMENTS

I would like to express sincere gratitude to my research supervisor Assoc. Prof. Dr. Açelya YILMAZER AKTUNA, for giving me the opportunity to do research and providing unique guidance. I am grateful for the time and effort she has spent to improve my scientific experience.

I would like to thank my lab mentor, my colleague, Cansu GÜRCAN KARATEPE who shared her experience and guided me to succeed in my experiments. I am truly grateful that she was always instructive, insightful, and most importantly patient towards me. In addition, I wish to send my regards and appreciation to every member of Yılmazer Lab.

I would like to thank Prof. Dr. Kostas KOSTARELOS for kindly providing the necessary graphene oxide materials for this thesis.

I would like to thank Assoc. Prof. Dr. Fikret ARI and Asst. Prof. Dr. Mehmet Altay ÜNAL who kindly provided the laser cutting device, shared their experiences and guided me to succeed in my experiments.

I would like to acknowledge Ankara University Scientific Research Projects Coordination Unit for providing financial support within the scope of this thesis (Project Number: 22L0443001).

I would like to thank many times to my family for their support and guidance throughout my life.

Oğuzhan PANATLI
Ankara, August 2022

TABLE OF CONTENTS

LIST OF SYMBOLS

°C	Degree Celsius
cm	Centimeter
ml	Milliliter
mm	Millimeter
nm	Nanometer
µg	Microgram
µl	Microliter
µm	Micrometer

Abbreviations

0D	Zero-Dimensional
1D	One-Dimensional
2D	Two-Dimensional
3D	Three-Dimensional
ANOVA	Analysis of Variance
ATCC	American Type Culture Collection
CAD	Computer-Aided Design
CNC	Computer Numeric Control
CO_2	Carbon Dioxide
DMSO	Dimethyl Sulfoxide
DSA	Double-Sided Adhesive
FBS	Foetal Bovine Serum
G	Graphene
GBM	Graphene-Based Material
GO	Graphene Oxide
h	Hour
ID	Inner Diameter

IDE	Integrated Development Environment
ILM	Inverted Light Microscope
LDH	Lactate Dehydrogenase
l-GO	Large Graphene Oxide Flakes
OD	Outer Diameter
PBMC	Peripheral Blood Mononuclear Cell
PBS	Phosphate Buffered Saline
PDMS	Polydimethylsiloxane
PI	Propidium Iodide
PMMA	Poly(methyl methacrylate)
PS	Phosphatidylserine
PVP	Polyvinylpyrrolidone
rcf	Relative Centrifugal Force
ROS	Reactive Oxygen Species
rpm	Revolutions Per Minute
RPMI	Roswell Park Memorial Institute
s-GO	Small Graphene Oxide Flakes
USB	Universal Serial Bus
us-GO	Ultrasmall Graphene Oxide Flakes

LIST OF FIGURES

LIST OF TABLES

1. INTRODUCTION

Conventional cell culture consists of two types of cell culture: Two-dimensional (2D) cell culture that cells adhere to a surface and suspension cell culture (Anonymous 2020). Although conventional cell culture has significant good aspects such as established culture material and protocol, standardization and availability of assays, this method does not entirely reflect nuances of the *in vivo* cellular microenvironment (Halldorsson, Lucumi, Gómez-Sjöberg, & Fleming, 2015; Young & Beebe, 2010). Therefore, conventional cell cultures are insufficient to fully mimic *in vivo* conditions in experimental studies (Aslım & Koçancı, 2018). Three-dimensional (3D) cell culture (Kapałczyńska et al., 2018; Saydé et al., 2021) and microfluidic cell culture (Wu, Huang, & Lee, 2010) methods have gained popularity in order to overcome this unfavorable situation and better mimic *in vivo* conditions.

Microfluidic systems used to control and manipulate fluids through micrometer-sized channels are an alternative to conventional methods (Sattari, Hanafizadeh, & Hoorfar, 2020). These systems have recently become a valuable option in many fields (biomedical, food, chemistry, medicine, pharmacy, agriculture, etc.) owing to their great advantages such as low cost, fewer sample requirements and low energy consumption. (Düven, Çetin, & Kışla, 2018; İçöz, Akar, & Ünal, 2020). Microfluidics also helps control of cellular microenvironment and thereby *in vivo* conditions can be better mimic in experimental studies (Mehling & Tay, 2014).

Since graphene-based nanomaterials have important properties, their potential in biomedical and nanomedicine applications is being explored. The immune system plays a significant role in most of the applications with graphene-based nanomaterials in biomedical and nanomedicine. Additionally, research on the biocompatibility of graphene-based nanomaterials is ongoing; therefore, evaluation of the effects of these nanomaterials on the immune system is an important precondition. (Orecchioni, Ménard-Moyon, Delogu, & Bianco, 2016).

In the literature, there are studies that graphene-based nanomaterials used in conventional cell culture (K. Wang et al., 2011) and 3D cell culture (de Lázaro et al., 2021); however, there are few studies that the nanomaterials used in microfluidic cell culture.

In respect of these developments, the biocompatibility of graphene oxide (GO) was investigated within the scope of this thesis. The effect of different sizes of GO on Jurkat cells, which are immune cells, was examined in both static (conventional cell culture) and dynamic (microfluidic cell culture) environment.

2. LITERATURE SURVEY

2.1 Graphene and its derivates

Carbon is an element that is commonly found in nature. It is an unusual material that can be available in zero-dimensional (0D), one-dimensional (1D), two-dimensional (2D), and three-dimensional (3D) forms (Zhang et al., 2017). Graphene (G), which is an allotrope of carbon, has a honeycomb nanostructure. This hexagonal structure, which is formed by the bonding of carbon atoms that have sp^2 hybridized, is a 2D and single-atom-thick layer. (Bitounis, Ali-Boucetta, Hong, Min, & Kostarelos, 2013; Gürcan, 2018; Yang, Asiri, Tang, Du, & Lin, 2013). Graphene forms the building block of allotropes of carbon from 0D to 3D (Zhang et al., 2017).

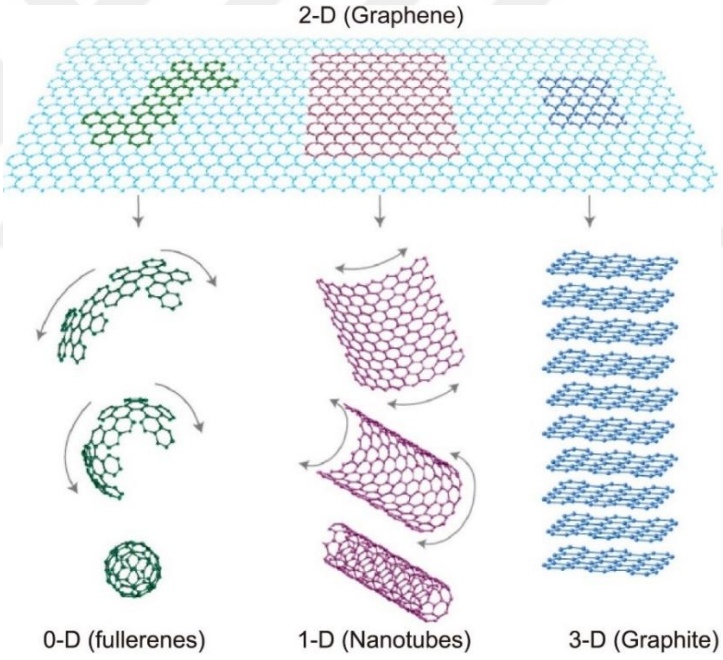

Figure 2.1 Illustration of various carbon allotropes (Zhang et al., 2017)

Graphene, which has extraordinary properties such as flexibility, lightness, high conductivity, and transparency, has become a popular material in many applications including flexible electronics (Eda, Fanchini, & Chhowalla, 2008), electrochemical biosensors (Du et al., 2010), tissue engineering (Menaa, Abdelghani, & Menaa, 2015), and medicine (Kostarelos, Vincent, Hebert, & Garrido, 2017).

Not only graphene but also graphene-based materials (GBMs) have become attractive today because of their potential to be used in many fields. Various GBMs are available, including single or multilayer G, graphene oxide (GO), graphene nanosheets and flakes, reduced graphene oxide, graphene nanoribbons, and GO quantum dots (Bianco, 2013; Cheng, Li, Thomas, Kotov, & Haag, 2017; Rizzo et al., 2018).

2.2 Graphene-based nanomaterials for biomedical applications

The potential of graphene-based nanomaterials in biomedical applications is being investigated due to their important properties (Qu et al., 2018). There are numerous researches conducted in the biomedical field with these materials to illustrate, antibacterial activity (Szunerits & Boukherroub, 2016), biosensing (Chung et al., 2013; Jung, Cheon, Liu, Lee, & Seo, 2010), bioimaging (Sun et al., 2008), cancer therapy, (Shen, Zhang, Liu, & Zhang, 2012), drug and gene delivery (Bao et al., 2011).

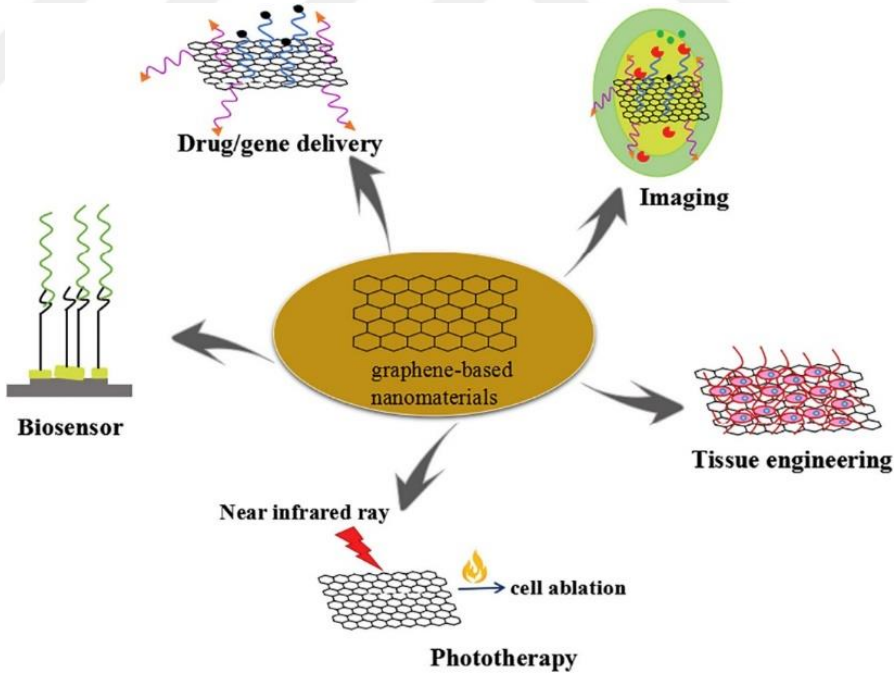

Figure 2.2 Fundamental applications of graphene-based nanomaterials in biomedical (Qu et al., 2018)

2.3 Graphene-based materials and immune cells

The immune system is a collection of molecules-cells and tissues that provides resistance to infections. The function of the immune system is to recognize molecules that are foreign to the body and destroy them (Karahan 2015).

As mentioned in the previous section, graphene-based (nano)materials have remarkable potential in biomedical applications. Drug and gene delivery, bioimaging, and anticancer therapy, for instance. Some of these studies in biomedical applications necessity intravenous injection of graphene and the assessment of its immune impact is a necessary precondition (Orecchioni, Ménard-Moyon, Delogu, & Bianco, 2016). In addition, the production and use of graphene-based nanomaterials has increased. That's why, it is necessary and important to carefully examine the effect of such nanomaterials on cells and tissues (Mukherjee, Bottini, & Fadeel, 2017).

Many studies have been conducted on the interaction of GBMs with immune cells. In most of the current studies, it is reported that GBMs interact with immune cells and can trigger situations, which leads to different effects on the body (Mukherjee, Bottini, & Fadeel, 2017).

The toxicity/compatibility of GBMs relies on various physicochemical properties including form, dimension/size, and surface chemistry. (Fadeel et al., 2018). As summarized in figure 2.3, the majority (~80%) of research on immune effect were performed with GO. ~10% of the research were performed with pure G and ~10% with other forms of G (Orecchioni, Ménard-Moyon, Delogu, & Bianco, 2016).

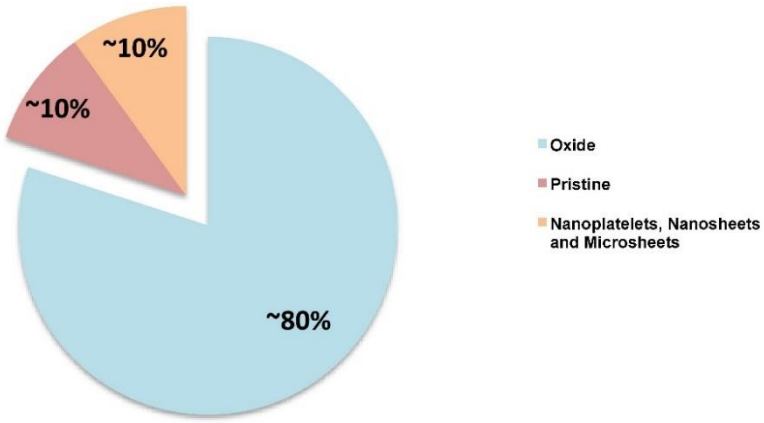

Major findings

Different types of graphene studied	Toxic	Non toxic	Activation	No activation
Shape dimension <1um	2	3	4	2
Shape dimension ≥1um	4	5	2	4
Aminated	1	0	1	0
Polyvinylpyrrolidone	0	1	1	0
Carboxylated	1	1	2	0
Carboxylated and PEGylated	0	1	1	0
PEGylated and polyethyleniminated	0	1	1	0
PEGylated	0	2	0	2
Ovalbumin and carnosine	0	1	1	0
Peptide (Vpr13-33)	0	1	1	0
Pristine	3	0	3	0
Nanoplatelets	1	0	1	0
Nanosheets	1	0	1	0
Microsheets	1	0	0	0

Figure 2.3 Studies on immune effect conducted with graphene and its forms (Orecchioni, Ménard-Moyon, Delogu, & Bianco, 2016)

2.4 Biocompatibility of graphene-based nanomaterials

Members of GBMs do not have a uniform surface. Pristine G surface has hydrophobic; on the other hand, GO surface has hydrophobic islands with hydrophilic regions. This might potentially affect the interactions of these materials with biological systems (Mukherjee, Bottini, & Fadeel, 2017). In many papers, it has been reported that GO shows better immune compatibility compared to pristine G (Orecchioni, Ménard-Moyon, Delogu, & Bianco, 2016).

Russier et al. (2013) stated that the different GO sheet sizes (~1.32 μm, ~0.27 μm, and ~0.13 μm) caused an important effect on various cellular parameters including cellular viability, reactive oxygen species (ROS) generation, and cellular activation. The researchers showed that as the lateral dimensions of GO decreased, the effects on cellular internalization and cellular functionality increased.

Orecchioni et al. (2016) examined the immunotoxicological effect of GOs with two different sizes on human peripheral blood mononuclear cells (PBMCs). They demonstrated that small sized GO induced a more prominent effect on immune cells compared to large sized GO.

Zhi et al. (2013) studied the impact of surface modification on human immune cells and examined the effect of pure GO and polyvinylpyrrolidone (PVP) coated GO. In short, the researchers reported that coating with PVP may clearly improve the in vitro immunological biocompatibility of GO.

As discussed above, after exposure, graphene-based (nano)materials may be detected by immune cells. Studies continues on various methods, including surface modification, to perfom these nanomaterials more compatible. On the other hand, a coherent contemporary approach to classify these nanomaterials based on their immune properties other than their physicochemical parameters is lacking (Gazzi et al., 2020). For this reason, it is thought that studies should be done on the interaction between immune cells and graphene-based materials.

2.5 Microfluidics

Microfluidics is the engineering of systems that precisely control and manipulate small volumes of fluids through micrometer-sized channels (Nguyen, Wereley, & Shaegh, 2019; Whitesides, 2006). Over the last few decades, this technology has grown rapidly. Due to the fact that microfluidic devices have remarkable advantages such as less analytes and reagents, precise fluid control, fast, low cost, or no need for specialist staff, there are a number of potential applications for these devices in various research fields,

including biomedical, pharmacy, chemistry, food, information technology, optics, medicine, agriculture (Akar, 2020; Düven et al., 2018; McDonald et al., 2000).

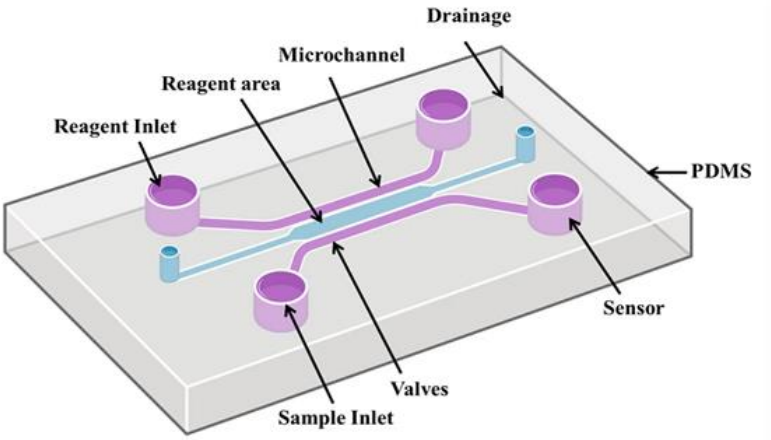

Figure 2.4 Illustration of a microfluidic chip (Pattanayak et al., 2021)

Nowadays, microfluidic systems have become an important option in many research areas including biomedical, pharmacy, chemistry, food, medicine, agriculture owing to remarkable advantages such as (Akar, 2020; Düven et al., 2018; McDonald et al., 2000):

- consumption of less analytes and reagents,
- precise control of liquids,
- reduction in analysis time,
- low cost of fabrication, usage, and disposal,
- easy portability,
- no need for specialist staff.

2.6 Biomedical applications of microfluidic devices

Microfluidic devices have become a significant research area in biomedical engineering applications today. Microfluidic systems are used in various research including tissue engineering, cell culture, biosensors, cancer, discovery of new drug molecules (McDonald et al., 2000; Pattanayak et al., 2021).

Although conventional cell culture has significant good aspects such as established culture material and protocol, standardization and availability of assays, this method is insufficient to entirely mimic nuances of the *in vivo* cellular microenvironment. To address this limitation, microfluidic systems are used in cell culture applications. Microfluidic cell culture offers remarkable advantages compared to conventional cell culture. Comparison of conventional and microfluidic cell cultures are given in table 2.1 (Halldorsson et al., 2015; Mark, Haeberle, Roth, Stetten, & Zengerle, 2010).

Table 2.1 Advantages and drawbacks of conventional and microfluidic cell cultures

	Conventional Cell Culture	**Microfluidic Cell Culture**
Typical Advantages	➢ Established culture material, ➢ Standardized measurement of pH, CO_2, O_2, ➢ Established culture protocols, ➢ Standardization and availability of assays, ➢ Ability to scale up single experiment	➢ Less use of laboratory space, ➢ Automation, ➢ Cost effective, ➢ Using fewer cells, ➢ Experimental flexibility and control
Typical Drawbacks	➢ Fixed device architecture, ➢ Perfusions and chemical gradients are difficult to archive, ➢ Stagnant culture media, ➢ Rigid culture surface, ➢ Mainly end-point analysis	➢ Relatively new technology, ➢ New culture surface like PMMA, ➢ Complex operational control and chip design, ➢ Non-standard culture protocols

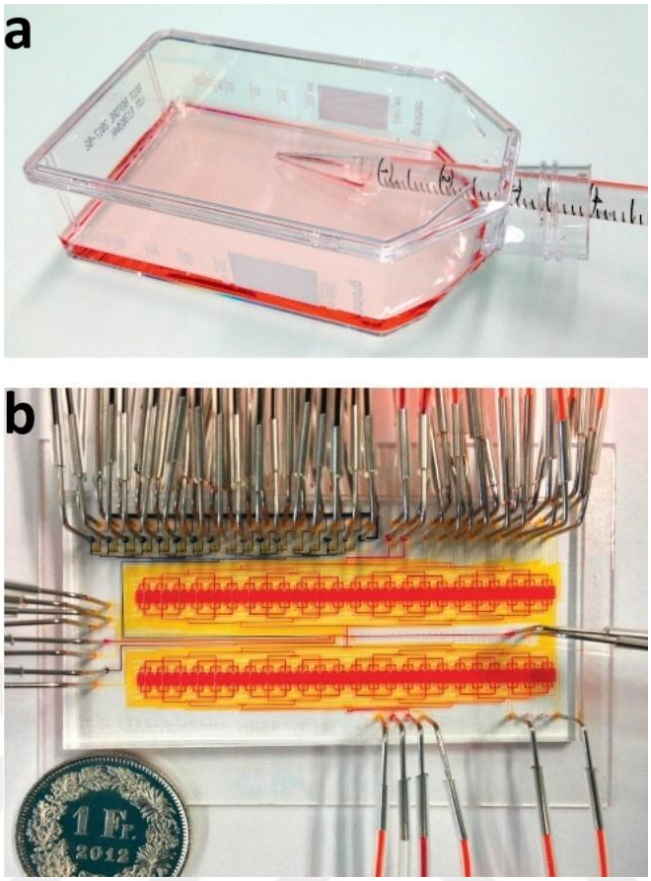

Figure 2.5 Cell cultures, (a) conventional cell culture, (b) microfluidic cell culture (Mehling & Tay, 2014)

2.7 Materials for microfluidic chip fabrication

One of the first and most important steps in microfluidic applications is to determine the right material for chip fabrication. The type of material may vary depending on the applications, so it is necessity to consider the properties of the material to be used in chip fabrication. A number of materials have been used in chip fabrication over the past two decades. Microfluidic chips may be produced today with a variety of materials to illustrate, glass and silicone, Polydimethylsiloxane (PDMS), Poly(methyl methacrylate) (PMMA), paper (Niculescu, Chircov, Bîrcă, & Grumezescu, 2021; Ren, Zhou, & Wu, 2013).

Silicon or glass was used in the first-generation microfluidic chips. These materials are very reliable, but the method, which is called standard photolithography, used for the

fabrication of chips is quite costly. In the following years, PDMS began to be used in the production of microfluidic chips. PDMS is an elastomer which is used in chip fabrication. PDMS is the most popular material among elastomers in microfluidic fields. It has important advantages such as high biocompatibility, gas permeability, high flexibility, and transparency. Apart from PDMS, one of the most preferred materials is PMMA which is a thermoplastic. PMMA has important features such as transparency, inexpensive, availability, easy to pattern. PMMA has a disadvantage in long-term cell studies because of the fact that it barely allows gas permeability. Paper-based microfluidic chips are used in different applications like pregnancy testing. Paper is one of the suitable substrates in different microfluidic applications due to its properties including user-friendly, cheap, disposable. Some types of materials used in microfluidic chip fabrication and their properties are demonstrated in figure 2.6 (Mou & Jiang, 2017; Ren et al., 2013).

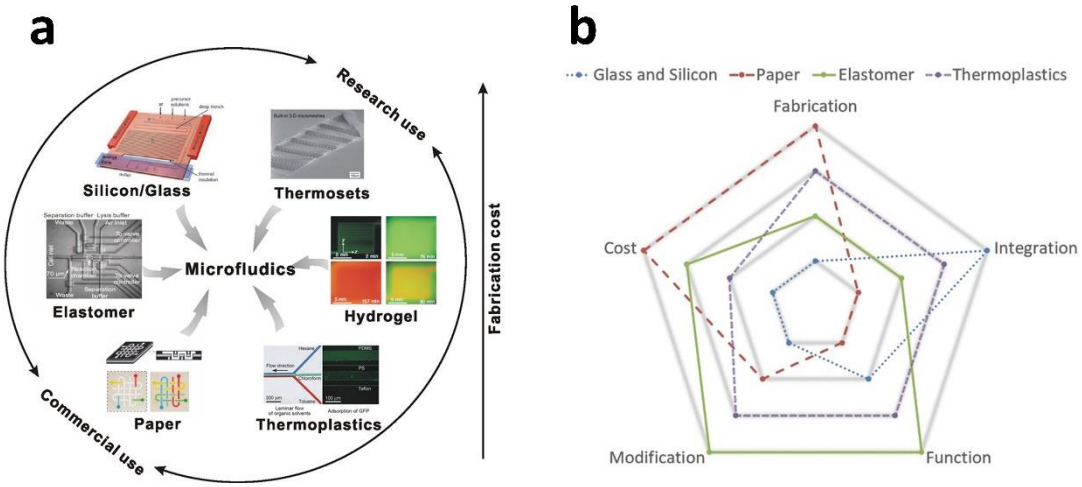

Figure 2.6 Different types of materials used in microfluidic chip fabrication (Mou & Jiang, 2017; Ren et al., 2013)

2.8 Microfluidic chip fabrication methods

Besides using different materials, different fabrication methods are used in microfluidic chips today. Soft lithography, laser ablation, and 3D printing methods are some of the fabrication methods (Niculescu et al., 2021). In the soft lithography method, briefly, a mold that has chip design is formed. PDMS, which is a suitable material in this method,

is poured onto the mold. Hardening of the PDMS is provided. After that, the PDMS forming the chip channels is removed from the mold and adhered to glass bottom layer (McDonald et al., 2000; Özbey, 2011).

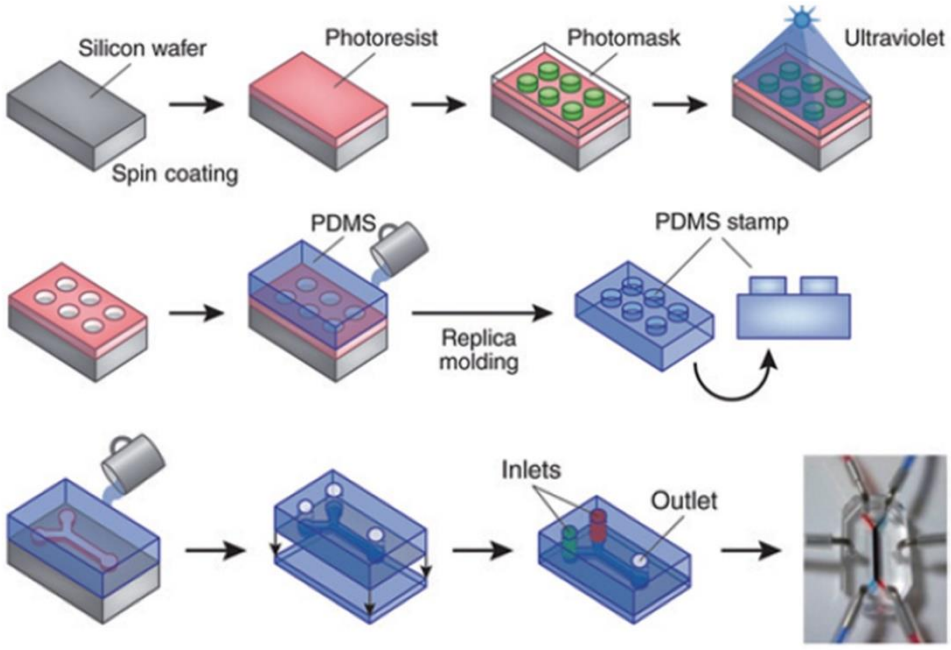

Figure 2.7 PDMS chip fabrication (Z. Wang et al., 2015)

In laser-based processes, in short, the designed microfluidic chip can be fabricated by laser engraving or cutting. In laser cutting method, PMMA, double-sided adhesive (DSA) and glass are among the most preferred materials as top, middle and bottom layers, respectively. In this method, a basic microfluidic chip consists of 3 layers. PMMA is the top layer with inlet and outlet. DSA is the middle layer which has microchannel geometry. The bottom layer is glass. These three layers are assembled with careful attention to alignment and the microfluidic chip is fabricated (Niculescu et al., 2021).

2.9 Microfluidic chip designs

Microfluidic chip designs can vary according to different applications, including lab-on-a-chip, organ-on-a-chip, tumor-on-a-chip, cancer-on-a-chip, single-cell analysis, drug screening in addition to material or fabrication method (Pattanayak et al., 2021).

Schematic illustration of different channel geometries is demonstrated in figure 2.8 (Carvalho, Ceccato, Michelon, Han, & de la Torre, 2022; Damiati, Kompella, Damiati, & Kodzius, 2018).

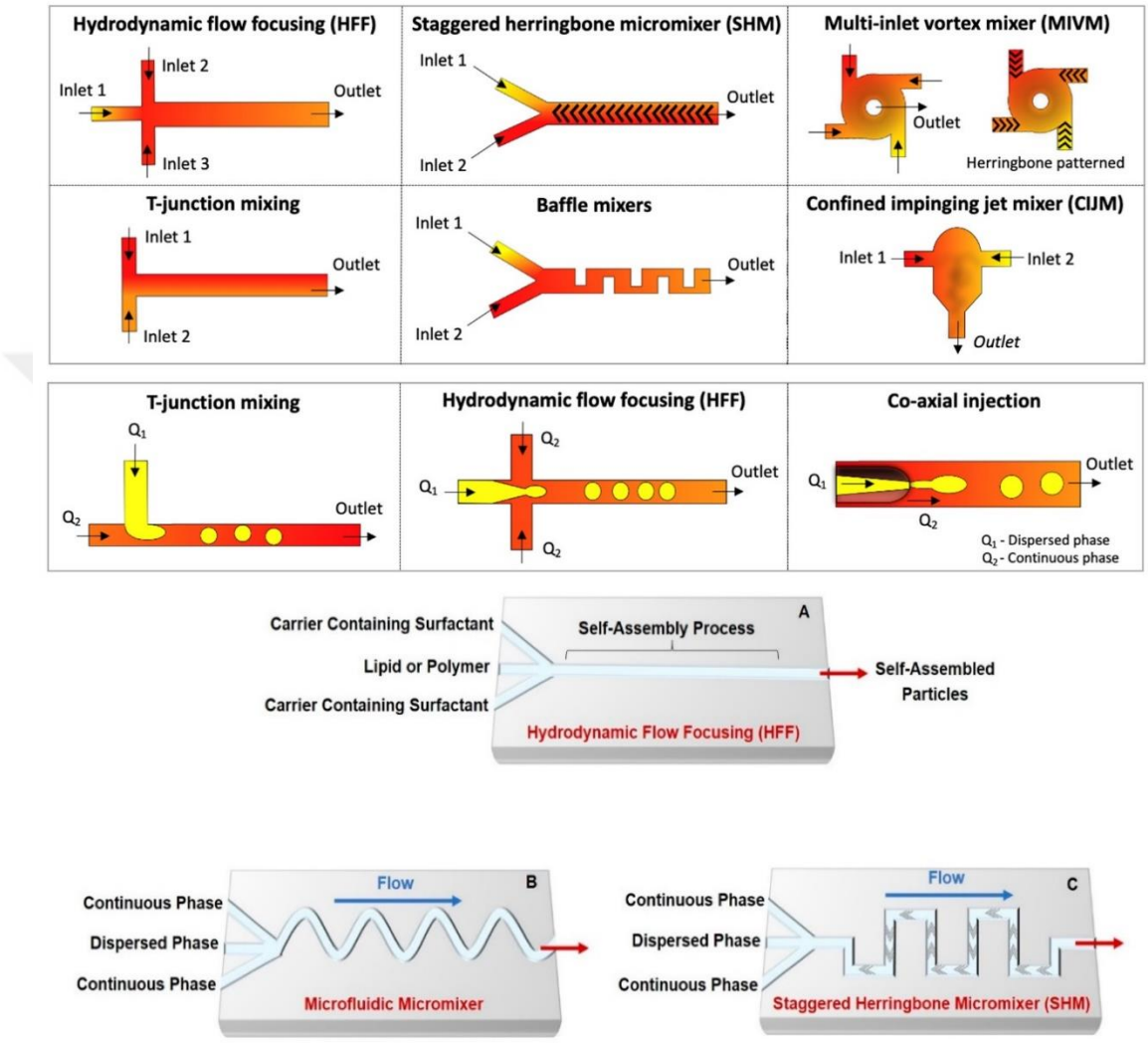

Figure 2.8 Different microfluidic chip designs (Carvalho, Ceccato, Michelon, Han, & de la Torre, 2022; Damiati, Kompella, Damiati, & Kodzius, 2018)

Comprehension of immune system is very significant in biomedical applications, such as drug development research, implant design. Conventional cell cultures and animal models are frequently used in these applications. However, conventional cell cultures or animal models suffer from at least one challenge, such as the inability to fully mimic cellular microenvironment, ethical concern, need for specialist staff, high cost. Research conducted with microfluidic chip technology has gained momentum in order to

overcome these unfavorable situations. Microfluidic chips with immune cell components are given in figure 2.9 (Morsink, Willemen, Leijten, Bansal, & Shin, 2020).

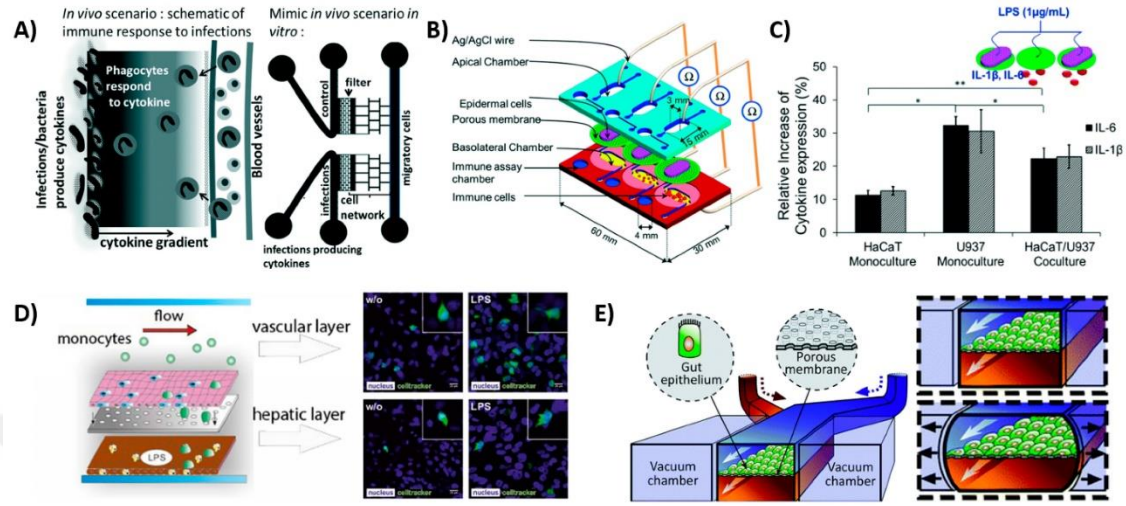

Figure 2.9 Microfluidic chips with immune cell components (Morsink, Willemen, Leijten, Bansal, & Shin, 2020)

2.10 Scope and novelty of the study

In this thesis, the biocompatibility of GO was investigated. To this end, the effect of different sizes of GO on Jurkat cells, which are an immortalized line of human T lymphocyte cells, was investigated in both static (conventional cell culture) and dynamic (microfluidic cell culture) environments. Jurkat cells represent good models to study immune biocompatibility of nanomaterials (Orecchioni et al., 2014; Orecchioni et al., 2016; Thurnherr et al., 2009; Zamorina et al., 2021). In our best knowledge, this thesis is the first comparative study of GO with different sizes on these cells in suspension (static) and microfluidic (dynamic) cell cultures. It is thought that examining the cell-nanomaterial interaction in conventional and microfluidic cell cultures is important to understand the biocompatibility of GO with different sizes and the effect of the different cell culture media.

3. MATERIALS AND METHODS

3.1 Materials

The materials/software used within the scope of this study are shown involving their purposes and the companies/institutions provided them in table 3.1.

Table 3.1 Materials used, manufacturers and their intended use

Material/Software	Brand/Company/Institution	Intended Use
Microfluidic Chip Fabrication		
AutoCAD 2020	Autodesk	Chip design
PMMA	Forem Reklam	Chip fabrication
DSA	3M 7955MP	Chip fabrication
Microscope slide	ISOLAB	Chip fabrication
Dulbecco's Phosphate Buffered Saline	Biological Industries	Chip cleaning
Peristaltic Pump System		
Arduino IDE	Arduino	Control of the peristaltic pump system
C# programming language	Microsoft	Control of the peristaltic pump system
Arduino UNO R3	Arduino	Construction of the peristaltic pump system
Peristaltic pump module	Robotistan	Construction of the peristaltic pump system
Driver expansion board	CNC shield v3	Construction of the peristaltic pump system
Stepper motor driver	DRV8825	Construction of the peristaltic pump system

Table 3.1 Materials used, manufacturers and their intended use (continued)

***In vitro* Study**		
Cell Type		
Jurkat cell line	American Type Culture Collection (ATCC)	*In vitro* studies
Cell Culture Medium		
RPMI 1640 Medium (1X)	Gibco	Jurkat cells expansion medium
Foetal Bovine Serum (FBS)	Biological Industries	Jurkat cells expansion medium
Penicillin-Streptomycin Solution	Biological Industries	Jurkat cells expansion medium
Conventional and Microfluidic Cell Cultures		
us-GO	Manchester University, Nanomedicine Lab	Investigation of its effect in cell cultures
l-GO	Manchester University, Nanomedicine Lab	Investigation of its effect in cell cultures
Assays		
CyQuant LDH Cytotoxicity Assay	Thermo Fisher Scientific	Cell viability analysis
Annexin V, Alexa Fluor™ 488 conjugate	Thermo Fisher Scientific	Apoptotic cell analysis
Statistical Analysis		
GraphPad Prism 9.4	GraphPad Software, Inc.	Statistical Analysis

3.2 Methods

The experiments planned for this thesis study were carried out in the EGAL Laboratory of Electrical and Electronics Engineering Department, and the Stem Cell and Regenerative Medicine Research Laboratory of Biomedical Engineering Department of Engineering Faculty of Ankara University. The laser cutting device which was used in

microfluidic chip fabrication process was kindly provided by Dr. Fikret Arı and Dr. Mehmet Altay Ünal, Ankara University faculty members. The us-GO and l-GO, which was reported that the lateral dimension to be less than 500 nm and 1-30 μm, respectively (Rodrigues et al., 2018), used in this thesis study were kindly provided by Dr. Kostas Kostarelos, University of Manchester Nanomedicine Lab. coordinator and the characterization of the GOs was done by Orecchioni et al (Orecchioni, Jasim, et al., 2016).

3.2.1 Microfluidic chip fabrication by laser cutting method

The method in the literature (Asghar et al., 2016; Gale et al., 2018) was followed for microfluidic chip fabrication. Microfluidic chips were fabricated by assembling three layers. A microscope slide was used as the bottom layer. A double-sided adhesive (DSA) that is a transfer tape was used as the middle layer. This layer also formed the chip channel. The top layer was a PMMA layer with inlet(s) and outlet. Microfluidic chips were produced in two different designs.

The microfluidic chips were designed using AutoCAD 2020 software and subsequently formed the top and middle layers using a laser cutter (Epilog Laser Mini 24). An Illustration of a simple microfluidic chip design is given in figure 3.1.

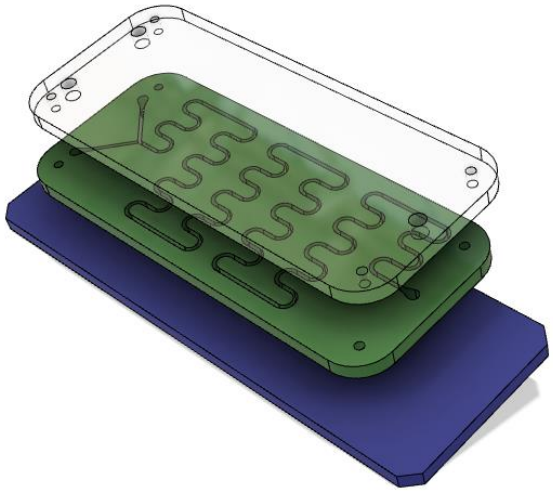

Figure 3.1 Illustration of a simple microfluidic chip design, top layer (PMMA), middle layer (DSA), bottom layer (microscope slide)

3.2.1.1 Bottom layer

The bottom layer was a standard microscope slide (75 mm x 26 mm) for both chips.

3.2.1.2 Middle layer

The middle layer was used to form channels. Channel geometry is an important factor in the interaction of fluids (Naher, Orpen, Brabazon, Poulsen, & Morshed, 2011); therefore, serpentine channels were designed to increase the mixing of fluids. CAD designs of the layer are demonstrated in figure 3.2 and figure 3.3.

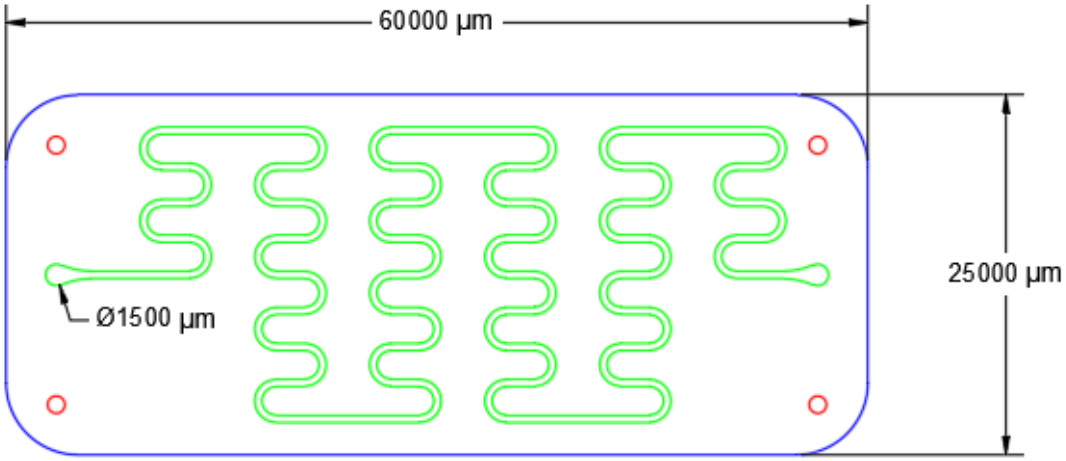

Figure 3.2 CAD design of middle layer (one inlet-one outlet)

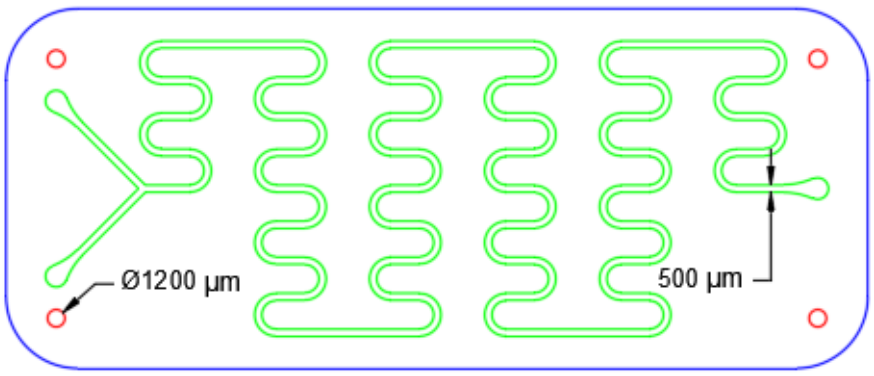

Figure 3.3 CAD design of middle layer (two inlets-one outlet)

The chip in figure 3.2 had one inlet and one outlet. Channel length was ~29 cm. Channel width was 500 µm. Channel volume was ~18.5 µl. The other chip (Figure 3.3) had two inlets and one outlet. Channel length was ~30 cm. Channel width was 500 µm. The channel volume was ~19.3 µl. The layer was patterned on DSA for both chips. The DSA thickness was 127 µm, which formed the channel height.

3.2.1.3 Top layer

The top layer was the layer with the input(s) and output ports of the chips. The top layer was designed to be compatible with the middle layer. PMMA was used as top layer. Transparent PMMA was preferred to see the fluid flow and its thickness was 2 mm. CAD designs of the layer are given in figure 3.4 and figure 3.5.

Figure 3.4 CAD design of top layer (one inlet-one outlet)

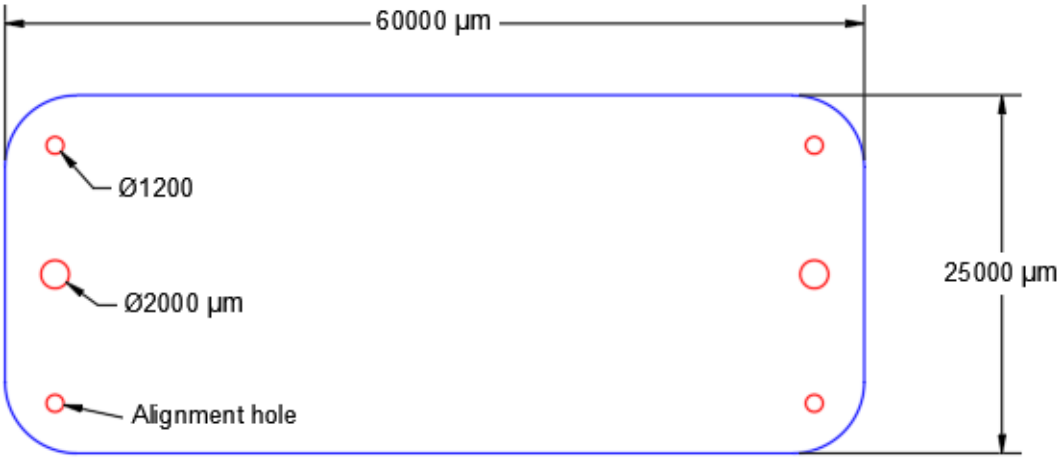

Figure 3.5 CAD design of top layer (two inlets-one outlet)

The inlet(s) and outlet diameters were 2 mm. The diameter of alignment holes was 1.2 mm.

The designed layers were cut using a laser cutter. Thus, top and middle layers were fabricated. Subsequently, top, middle, and bottom layers were assembled together. In this process, firstly, non-adhesive film on one surface of DSA was removed. Next the top layer, which is PMMA, was adhered to the DSA. After that non-adhesive film was removed from the other surface of DSA and a microscope slide was adhered to this surface. This process was applied for both chip designs.

Figure 3.6 Assembled microfluidic chip (one inlet-one outlet)

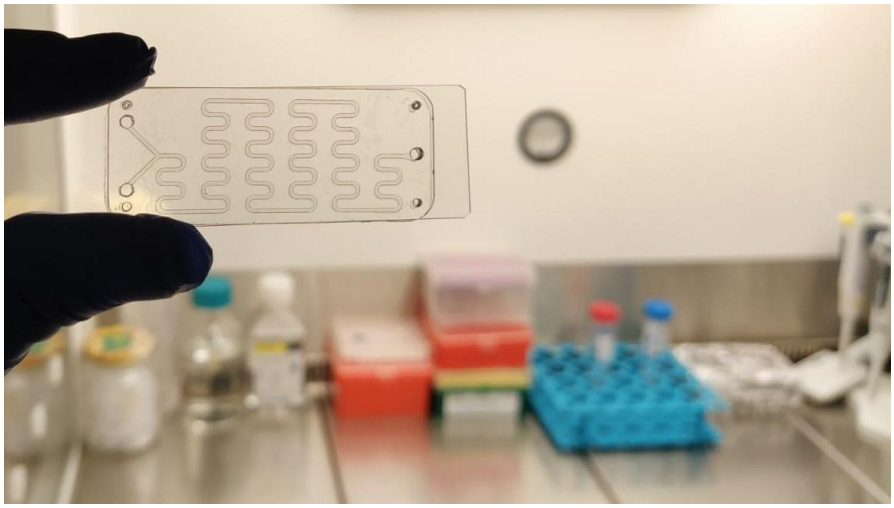

Figure 3.7 Assembled microfluidic chip (two inlets-one outlet)

3.2.2 Construction and control of the peristaltic pump system

3.2.2.1 Construction of the peristaltic pump system

As part of this thesis, it was presented a low-cost peristaltic pump constructed with common tools/hardware and open-source software.

The peristaltic pump system consisted of two basic parts: electrical-mechanical hardware and software. In the hardware part, there was a power supply, a microcontroller (Arduino UNO), a stepper motor driver (DRV8825), a driver expansion board (CNC shield), and a stepper motor-based peristaltic pump module. Schematic of the peristaltic pump system is given in figure 3.8.

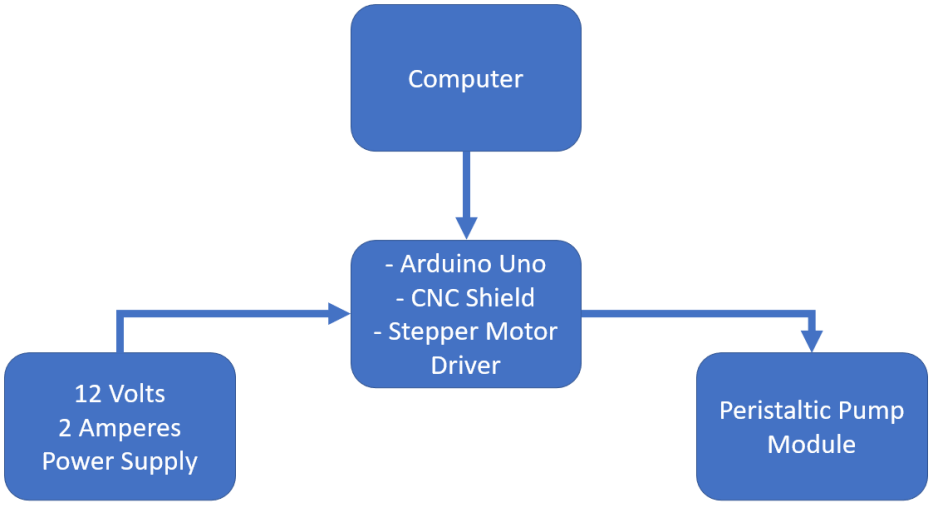

Figure 3.8 Schematic of the peristaltic pump system

In short, the Arduino microcontroller was responsible for sending commands that run the peristaltic pump and control the rotation speed of the peristaltic pump; nevertheless, this peristaltic pump could not work just by using Arduino. For this reason, CNC shield and stepper motor driver (DRV8825) were integrated to the Arduino. The peristaltic pump system is shown in figure 3.9. Wiring diagram of the peristaltic pump system is demonstrated in appendix 1.

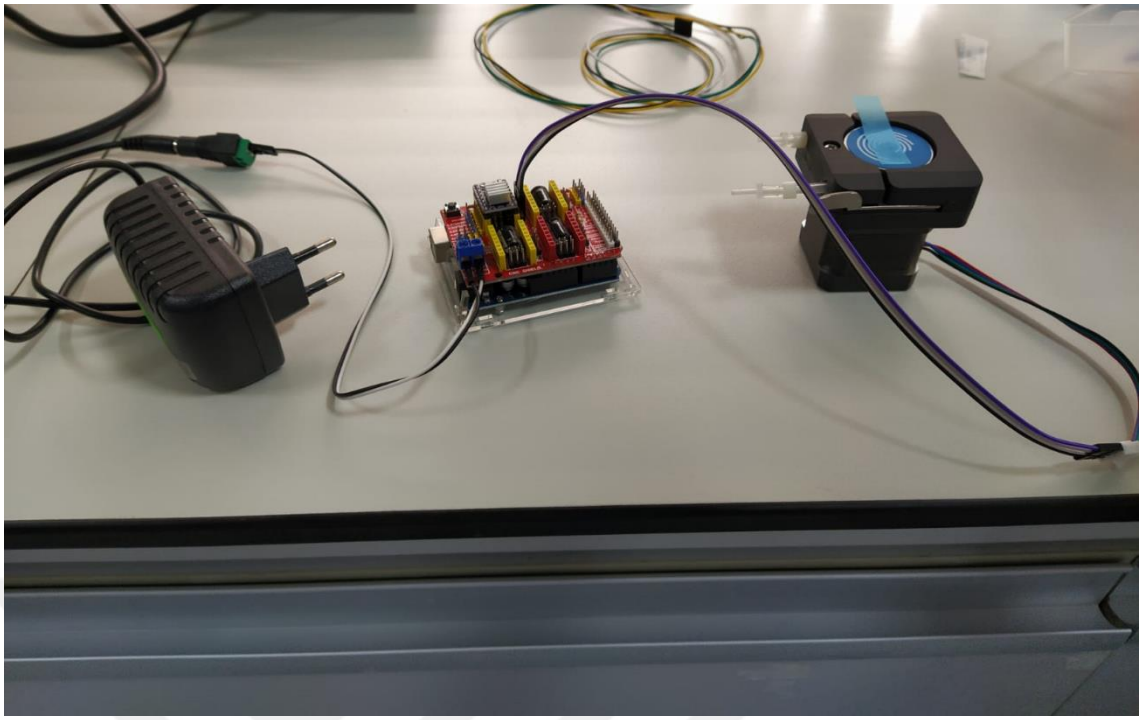

Figure 3.9 Peristaltic pump system. Arduino UNO, CNC shield, DRV8825, peristaltic pump module, power supply

3.2.2.2 Control of the peristaltic pump system

The Arduino microcontroller was programmed to control the peristaltic pump using the Arduino IDE, which is open-source software, through a USB connection to a computer. The Arduino IDE software is demonstrated in figure 3.10. Source code of the peristaltic pump system that was coded in Arduino IDE is in appendix 2.

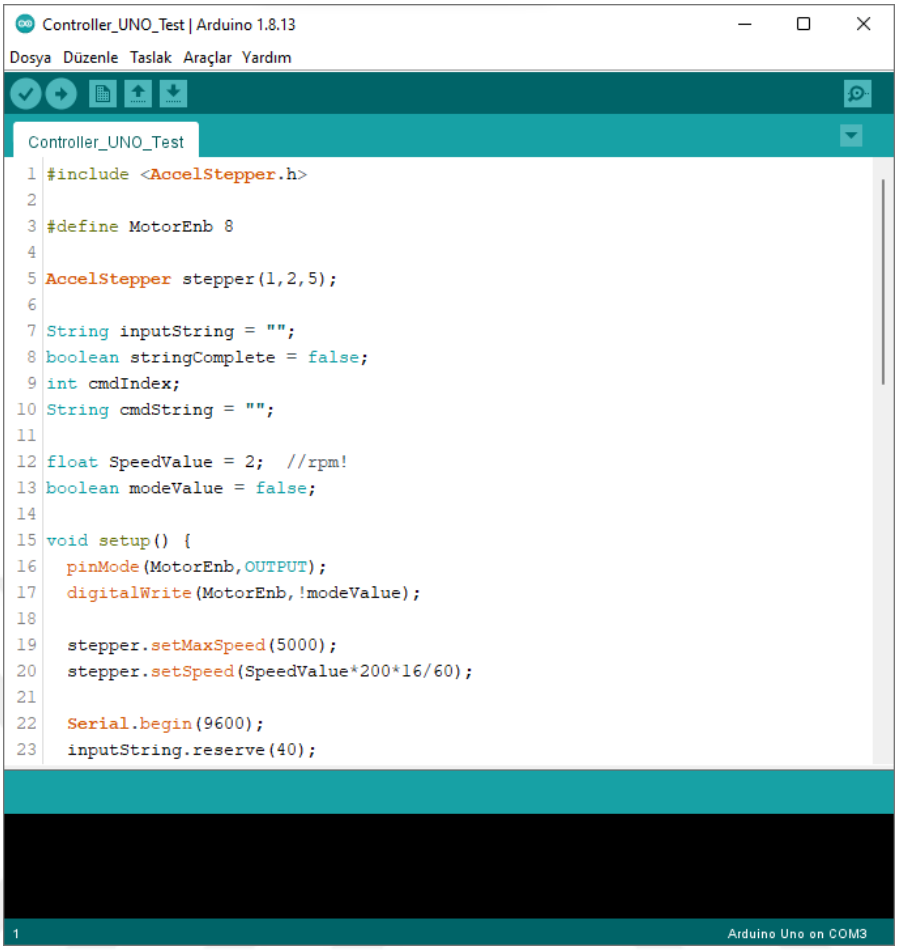

Figure 3.10 Arduino IDE

Although the peristaltic pump can be controlled from the serial port display of the Arduino IDE, there are some challenges in controlling it this way. For example, it may take some time to control more than one pump or change the speed of these pumps during experiments. A user-friendly, open-source peristaltic pump application was developed to prevent such challenges using C# programming language in Visual Studio 2019 IDE. Since this application had a simple and easy-to-use interface, peristaltic pumps were used together more effortlessly and comfortably (Figure 3.11). Source code of the peristaltic pump application is in appendix 3.

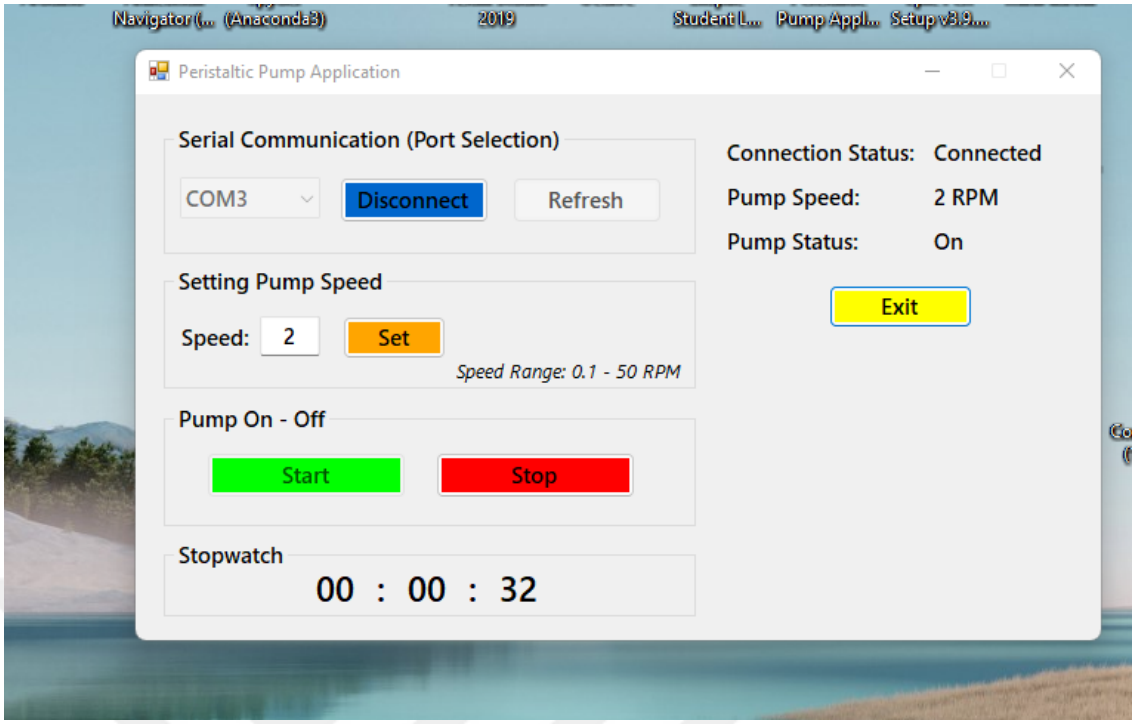

Figure 3.11 Peristaltic pump application

3.2.3 Fluid flow rate analysis

The flow rate test was carried out to determine rotation speed of the pump in µl/min. To perform the test, several revolutions per minute (rpm) values of the pump and two tubes of different diameters were used. The smaller diameter tubes were connected to both ends of the larger diameter tubing. Distilled water was passed through the pump at different rpms for one minute. After that the distilled water was collected in an eppendorf tube. The volume of fluid in the eppendorf tube was measured with a micropipette (Brand), and the rotation speed of the pump was calculated in µl/min.

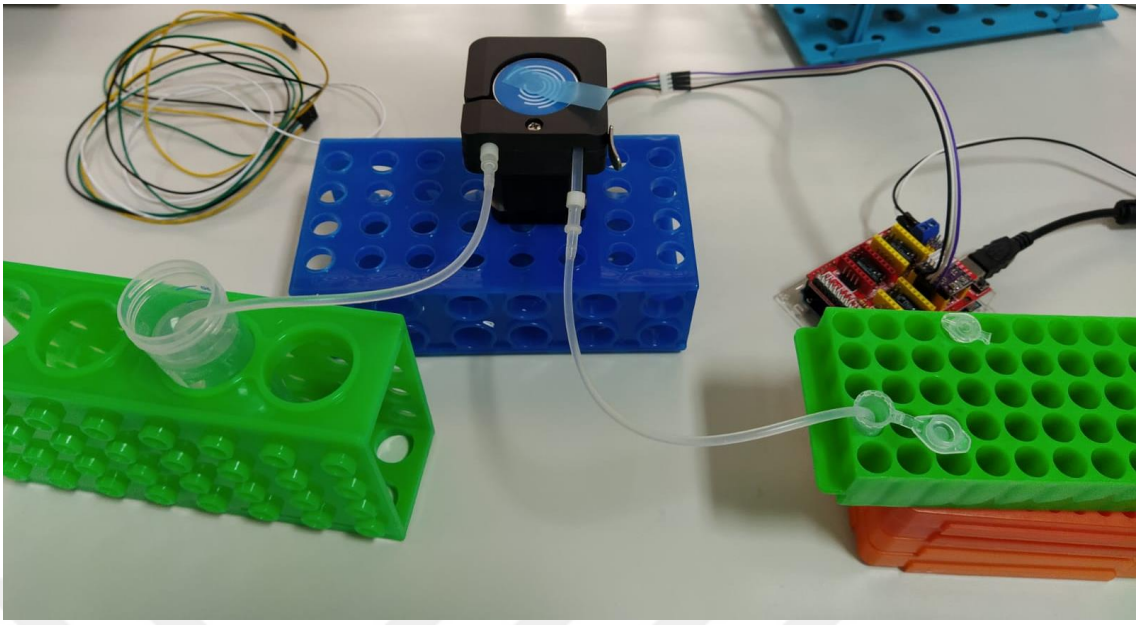

Figure 3.12 Flow rate test of peristaltic pump

3.2.4 Leakage analysis

The leakage test was carried out using medium to investigate whether there was a leakage. To perform the test, a microfluidic chip with microchannel geometry in figure 3.2 were used. After the microfluidic chips were fabricated, fittings were glued to the inlet and outlet holes with epoxy glue at room temperature so that the silicone tubing were connected microfluidic chip with the help of fittings. Utilizing a peristaltic pump, medium was passed through the microfluidic chip for 4 h at 0.5 rpm. Observation was carried out visually for any leakage in the microfluidic chip.

3.2.5 Occlusion analysis

The occlusion test was performed to investigate any possible occlusion using a microfluidic chip with microchannel geometry in figure 3.2. Medium with a volume of 1 ml and $5x10^5$ A549 lung cancer cells was used to perform the occlusion test. Jiang, Shen, and Piao (2010) reported that the diameter of A549 cells from two different microscopy images was 14.93 μm and 10.59 μm. Utilizing a peristaltic pump, the medium that contains the cells was passed through the microfluidic chip at 0.5 rpm for 2 h. Observation was carried out visually for any occlusion in the microfluidic chip.

3.2.6 *In vitro* studies

3.2.6.1 Preparation of cell culture

Jurkat cell line, which is defined an immortalized T lymphocyte cell line (Montano, 2014), was used within the context of this thesis. The cell line was obtained commercially from ATCC. The passage number and culture medium ingredient of this cell line are shown in detail in table 3.2.

Table 3.2 Cell type, passage number and cell medium ingredient

Passage Number	Cell Line	Cell Type	Medium Ingredient
4	Jurkat Cell Line	Jurkat	RPMI 1640 + 10% FBS + 1% Penicillin-Streptomycin

In the literature, there are studies with Jurkat cells on both conventional cell culture (Vashishtha, Nazarali, & Dimmock, 1998; Zamorina et al., 2021) and microfluidic device (Lee, Kim, Doh, Kim, & Chung, 2021; Metto et al., 2013). As Jurkat cells were studied in both conventional and microfluidic environments, these cells were used in the scope of the thesis. In order to culture Jurkat cells, A class II (laminar flow) biological safety cabinet (Labogene Mars) that its sterilization is provided by ultraviolet light was used. For Jurkat cells, the medium was prepared by adding 10% foetal bovine serum (FBS) and 1% penicillin-streptomycin into RPMI 1640 Medium (1X).

First, the Jurkat cells were removed from the tank which had liquid nitrogen in it. Secondly, the cells were thawed in a water bath at 37°C (little ice left in it). 2 ml of medium and thawed cells were collected into a falcon tube using a serological pipette. The volume of the solution was completed to 5 ml with the appropriate medium. The falcon tube was centrifuged at 260 rcf for 5 minutes to remove Dimethyl Sulfoxide (DMSO), which could cause toxic effects, from the cells. Then the supernatant was removed from these cells. Pelletized cells were removed by gentle tapping. The removed pellet was suspended with the appropriate volume of medium. Subsequently, the cells were seeded in a T-75 tissue culture flask for expansion. The necessary

medium was added to the flask. Afterwards, this flask was put in an incubator (Panasonic MCO-170AICUV-PE). Thus, the cells were incubated under appropriate conditions (37°C and 5% CO_2) in the incubator.

Figure 3.13 Steps of thawing and incubation of cells

3.2.6.2 Passaging of Jurkat cells and cell counting

After desired number of cells in the flask were achieved, cultured cells were passaged to ensure cell viability and remove metabolic wastes. Cells were counted to determine the appropriate cell densities in the studies.

For cell counting, the cultured cells were collected into the appropriate falcon tube. The cells that are in the falcon tube were centrifuged at 800 rpm for 5 minutes. After centrifugation the supernatant was removed from the tube. Next pelletized cells were removed by gentle tapping. The removed pellet was suspended with the appropriate volume of medium. 10 µl of the cell suspension was placed on the hemocytometer slide for cell counting and cells were counted under an inverted light microscope (ILM) (Zeiss).

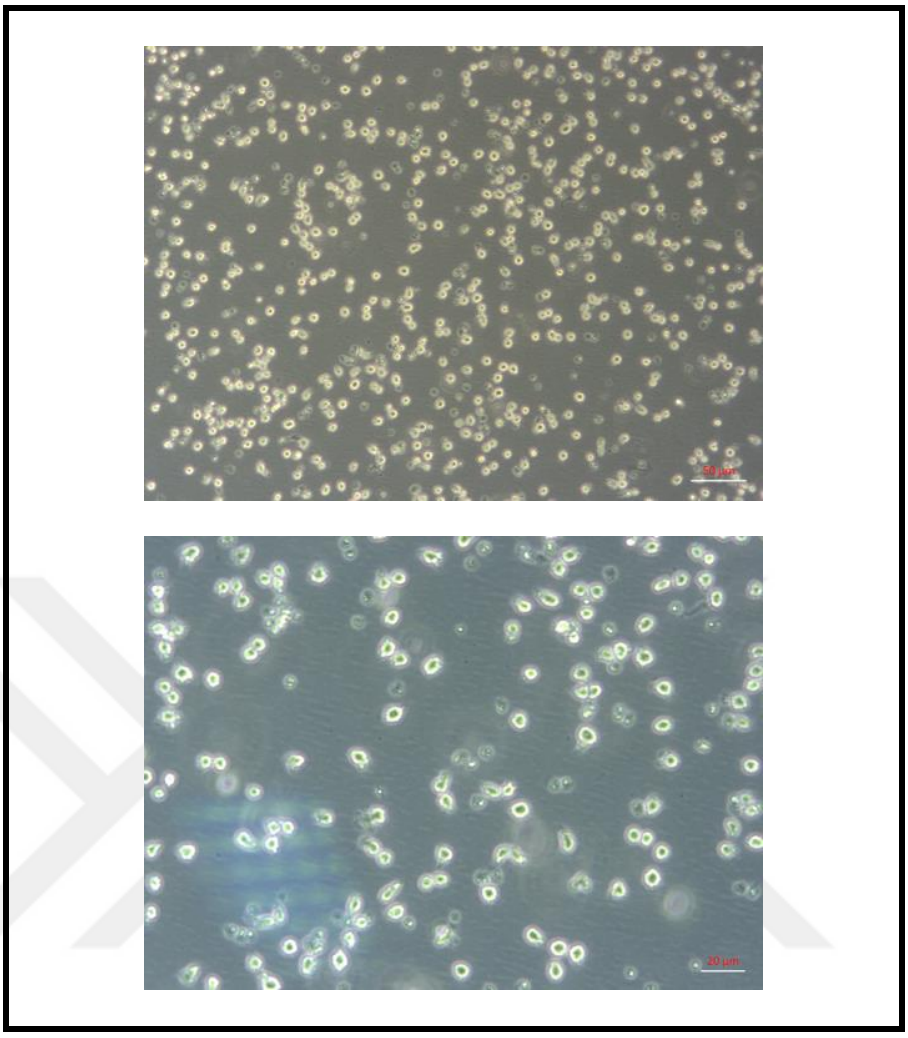

Figure 3.14 ILM images of Jurkat cells (10X and 20X magnifications)

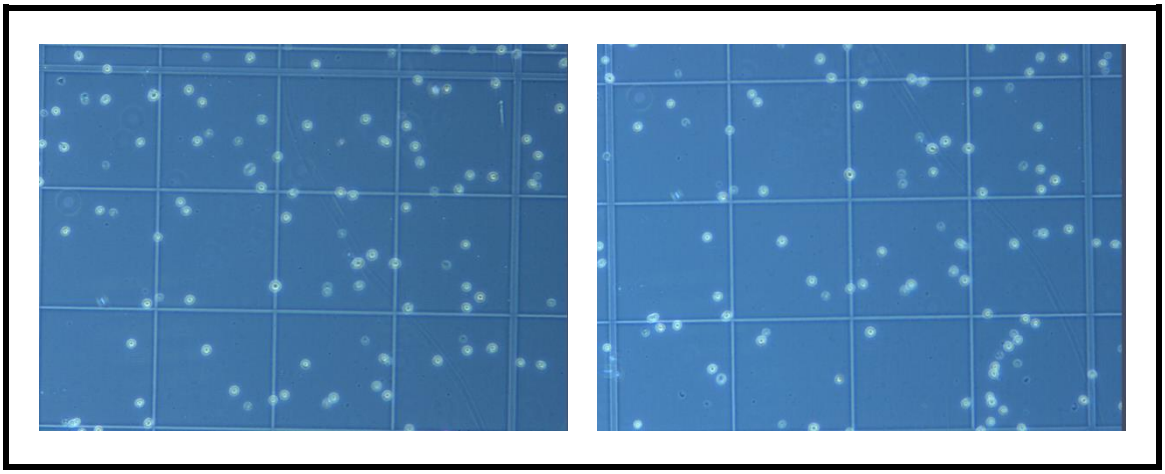

Figure 3.15 ILM images of Jurkat cells on hemocytometer slide (10X magnification)

3.2.6.3 The proliferation of Jurkat cells in conventional cell culture

After the cells were counted, the appropriate volume of medium that contains cells was prepared. The prepared medium was dispensed into 5 wells of 96-well plate. 200 µl of the medium was added per well. Thus, Jurkat cells were seeded at a density of ~$5x10^3$ cells/well in the 96-well plate. Then, the cells were incubated at 37°C, 5% CO_2 for 24 h. This cell culturing process was applied for LDH (Lactate dehydrogenase) assay.

For apoptosis assay, the appropriate volume of medium that contains cells was prepared. The Jurkat cells were seeded in a 6-well plate. Under the right conditions, the cells were incubated for 24 h.

3.2.6.4 The proliferation of Jurkat cells treated with us-GO in conventional cell culture

After the cells were counted, the appropriate volume of medium that contains cells was prepared. Afterwards us-GO, which was reported that the lateral dimension to be less than 500 nm (Rodrigues et al., 2018), with concentration of 100 µg/ml was added to the medium. In order to evenly mix the nanomaterial in the medium, the "up and down" technique was applied using a micropipette. The new medium was dispensed into 5 wells of 96-well plate. 200 µl of the medium was added per well, so Jurkat cells with a density of ~$5x10^3$ cells/well were seeded in the plate. Under favorable conditions, the cells were incubated for 24 h. This cell culturing process was applied for LDH assay.

For the apoptosis assay, the appropriate volume of medium that contains cells was prepared. Afterwards, us-GO with concentration of 100 µg/ml was added to the medium. Similar steps were followed, and the cells were incubated with the new medium (medium + nanomaterial) in a 6-well plate for 24 h under favorable conditions.

3.2.6.5 The proliferation of Jurkat cells treated with l-GO in conventional cell culture

After the cells were counted, the appropriate volume of medium that contains cells was prepared. Then l-GO, which was reported that the lateral dimension to be 1-30 μm (Rodrigues et al., 2018), with concentration of 100 μg/ml was added to the medium. In order to evenly mix the nanomaterial in the medium, the "up and down" technique was applied using a micropipette. The new medium was dispensed into 5 wells of 96-well plate. 200 μl of the medium was added per well, so Jurkat cells with a density of ~$5x10^3$ cells/well were seeded in the plate. Under the right conditions, the cells were incubated for 24 h. This cell culturing process was applied for LDH assay

For the apoptosis assay, the appropriate volume of medium that contains cells was prepared. Afterwards, l-GO with concentration of 100 μg/ml was added to the medium. Similar steps were followed, and the cells were incubated with the new medium (medium + nanomaterial) in a 6-well plate at 37°C, 5% CO_2 for 24 h.

3.2.6.6 The proliferation of Jurkat cells in microfluidic cell culture

Before starting the microfluidic cell culture, some pre-processing was carried out. Distilled water and alcohol were passed through the microfluidic chips and tubing, respectively. After that they were exposed to ultraviolet light for 1 h in a laminar flow cabinet. Lastly, phosphate buffered saline (PBS) was passed through the chips and tubing. Thus, the cleaning of microfluidic chips was carried out. After these procedures, the cell culture process was started.

After cells were counted, medium with a volume of 1 ml and $1x10^5$ cells was prepared. The prepared medium was transferred into a microfluidic chip using a peristaltic pump. A microfluidic chip with one inlet and one outlet was used (the chip design is shown in figure 3.1). Recirculation flow in the microfluidic chip was maintained using the peristaltic pump. Peristaltic pump speed was set to 0.5 rpm. Subsequently, the cells were incubated for 24 h under appropriate conditions (37°C, 5% CO_2). The flow in the

chip continued throughout the incubation. This cell culturing process was applied for both LDH and apoptosis assays.

3.2.6.7 The proliferation of Jurkat cells treated with us-GO in microfluidic cell culture

First, the pre-processes in the previous section were followed. Later a suitable volume of medium with $1x10^5$ cells was prepared. After that the appropriate volume of us-GO solution was prepared. The nanomaterial (us-GO) concentration was determined as 100 µg/ml. The total volume of the medium and nanomaterial solution was 1 ml.

The prepared medium and nanomaterial suspension were transferred to microfluidic chip from different channels using two peristaltic pumps. A microfluidic chip with two inlets and one outlet was used (the chip design is shown in figure 3.2). The medium and nanomaterials came together in the chip for the first time. Afterwards, this new medium (medium + nanomaterial) was transferred to a new microfluidic chip with one inlet and one outlet (Figure 3.1). Recirculation flow in the microfluidic chip was maintained using a peristaltic pump. Peristaltic pump speed was set to 0.5 rpm. Subsequently, the cells were incubated for 24 h under appropriate conditions. The flow in the chip continued during the incubation. This cell culturing process was applied for both LDH and apoptosis assays.

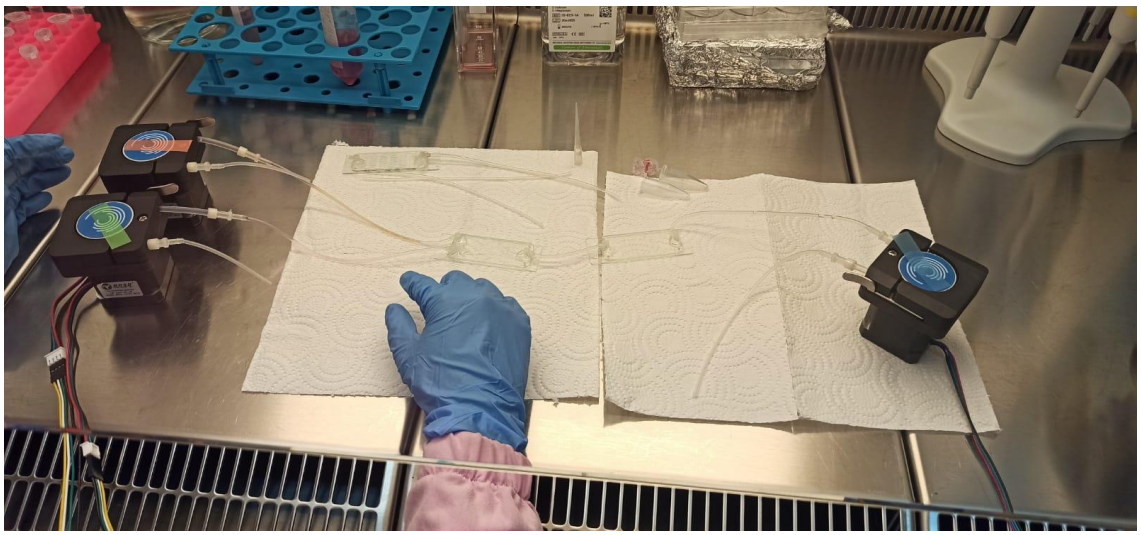

Figure 3.16 Simultaneous transfer of nanomaterial and Jurkat cells to microfluidic chip

3.2.6.8 The proliferation of Jurkat cells treated with l-GO in microfluidic cell culture

First, the pre-processes in the previous section were followed. Later a suitable volume of medium with $1x10^5$ cells was prepared. Afterwards, the appropriate volume of l-GO solution was prepared. The nanomaterial (l-GO) concentration was determined as 100 µg/ml. The total volume of the medium and nanomaterial solution was 1 ml.

The prepared medium and nanomaterial suspension were transferred to microfluidic chip from different channels using two peristaltic pumps. A microfluidic chip with two inlets and one outlet was used (the chip design is shown in figure 3.2). The medium and nanomaterials came together in the chip for the first time. Afterwards, this new solution (medium + nanomaterial) was transferred to a new microfluidic chip with one inlet and one outlet (Figure 3.1). Recirculation flow in the microfluidic chip was maintained using a peristaltic pump. Peristaltic pump speed was set to 0.5 rpm. Subsequently, the cells were incubated for 24 h under favorable conditions. The flow in the chip continued during the incubation. This cell culturing process was applied for both LDH and apoptosis assays.

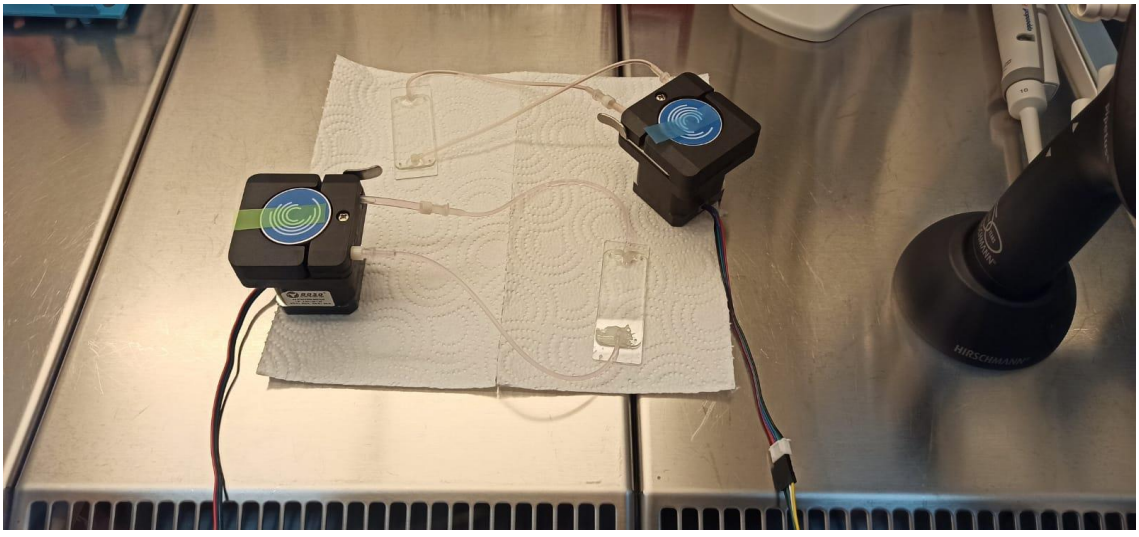

Figure 3.17 Recirculation flow in microfluidic chips using peristaltic pump

Cells in both static (conventional) and dynamic (microfluidic chip) media were cultured simultaneously. After the cells were incubated for 24 h, In order to analyze the viability of the cells, assays were performed.

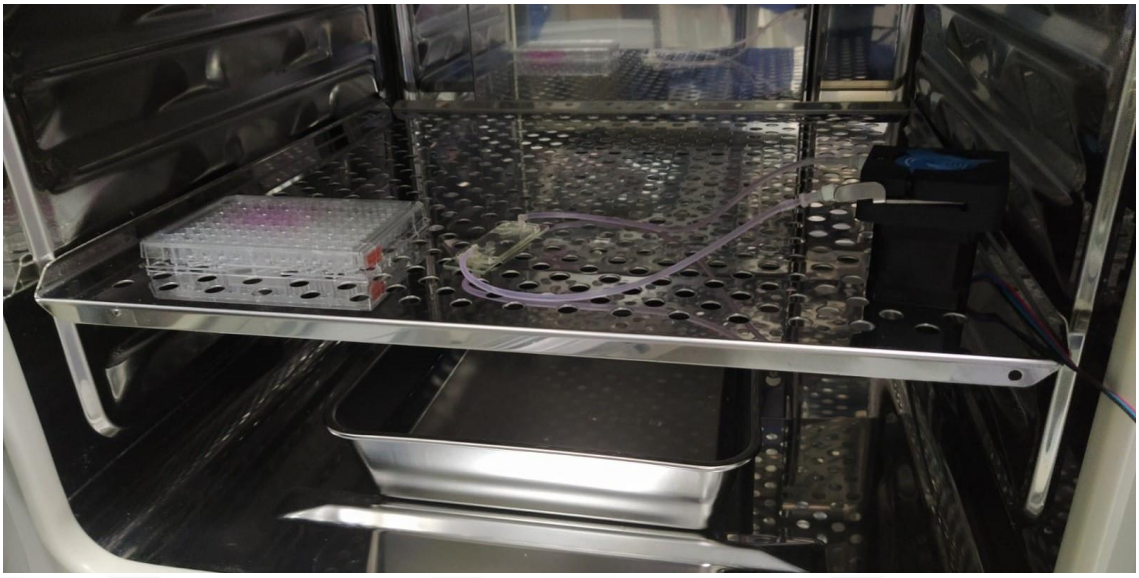

Figure 3.18 Conventional and microfluidic cell cultures (96-well plate and microfluidic chip)

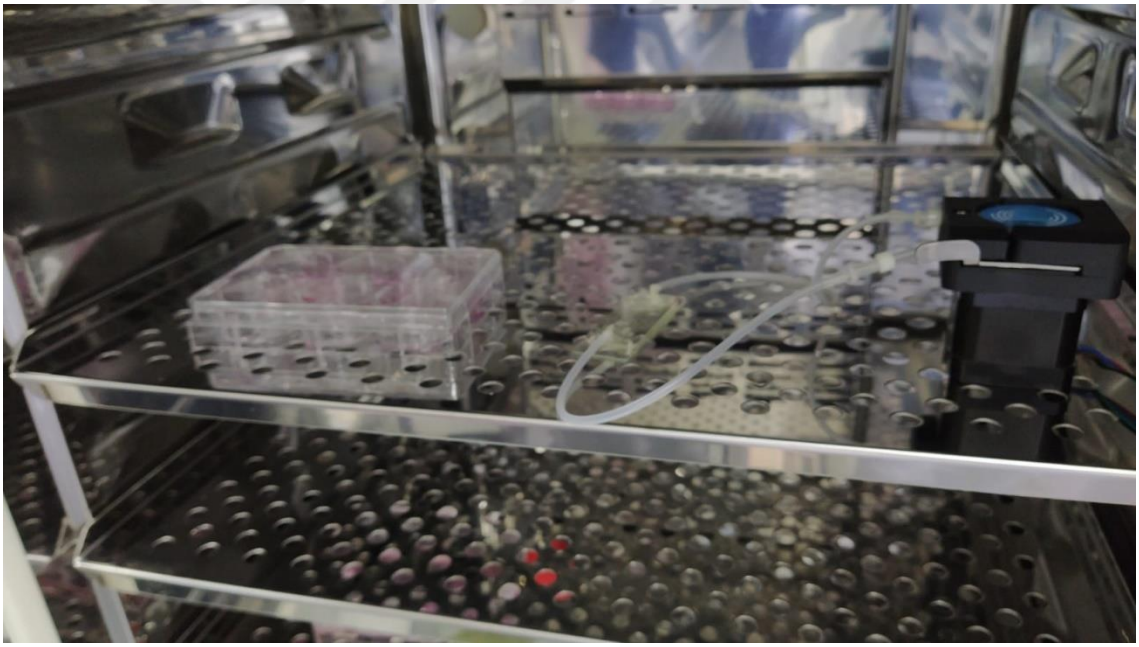

Figure 3.19 Conventional and microfluidic cell cultures (6-well plate and microfluidic chip)

3.2.7 LDH assay

Cytotoxicity assays occupy an important place in *in vitro* toxicology studies. LDH assay is one of the commonly preferred assays for detecting cell viability or cytotoxicity. (Fotakis & Timbrell, 2006).

Lactate dehydrogenase (LDH) is a cytoplasmic enzyme which is present in all cells (Erkekoğlu & Baydar, 2021; Kumar, Nagarajan, & Uchil, 2018). When cells are exposed to a toxic substance, their plasma membrane integrity is disrupted and LDH leaks from the cells into the cell medium. This is measured spectrophotometrically (Erkekoğlu & Baydar, 2021). LDH assay is reliable, rapid, and allows for simple evaluation (Fotakis & Timbrell, 2006).

Cell viability of the cells was assessed by LDH release. Cells incubated in conventional and microfluidic cell cultures for 24 h were removed from the incubator. For LDH assay, Jurkat cells in microfluidic cell culture were transferred to the 96-well plate, in which Jurkat cells in conventional cell culture were incubated. For this, the media with cells in the microfluidic cell culture was first collected into an eppendorf tube with the help of the peristaltic pump. The collected media was dispensed into 5 wells of 96-well plate. 200 µl of the media was added per well. This process was performed for all 3 media (Jurkat, Jurkat + us-GO, Jurkat + l-GO) in microfluidic cell culture. For the LDH assay, CyQuant LDH Cytotoxicity Assay Kit (Thermo Fisher Scientific) was used following the manufacturer's instructions.

Initially, 10 µl/well of lysis buffer was added and incubated at 37°C, 5% CO_2 for 45 minutes. Secondly, the cells were transferred to a falcon tube and centrifuged at 13000 rpm for 10 minutes. Then, the supernatant was dispensed into 50 µl/new wells. 50µL of Reaction Mixture was transferred to each sample well and mixed by gentle tapping. Subsequently, the plate was incubated at room temperature for 30 minutes protected from light. At the end of the incubation, 50µL of Stop Solution was added to each sample well and mixed by gentle tapping. Finally, the absorbance was measured at 490 nm and 680 nm in a microplate reader (Bmg Labtech CLARIOstar).

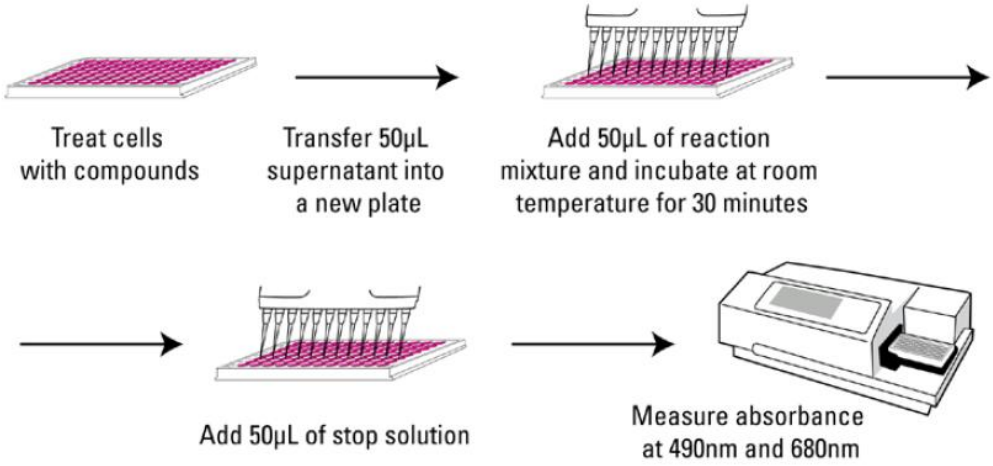

Figure 3.20 Schematic representation of LDH assay (Anonymous 2014)

3.2.8 Apoptosis assay

Apoptosis (programmed cell death) plays a major role in a number of cellular events (Koopman et al., 1994; Sgonc & Gruber, 1998). After cells signal apoptosis, they demonstrate some biochemical and morphological changes, for example, DNA fragmentation, cell shrinkage, chromatin condensation. These changes can be determined using a variety of methods (Güleş & Ülker, 2008). Schematic representation of apoptosis mechanism is given in figure 3.21 (Anonymous 2019).

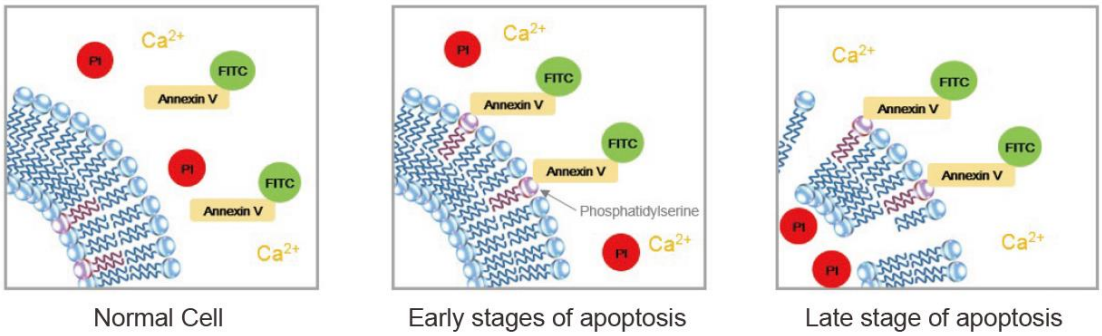

Figure 3.21 Schematic representation of apoptosis mechanism (Anonymous 2019)

For the apoptosis assay, The Alexa Fluor® 488 annexin V / Dead Cell Apoptosis Kit containing Alexa® Fluor 488 annexin V and Propidium iodide (PI) was used following the manufacturer's instructions. Briefly, Jurkat cells in conventional and microfluidic

media were washed 3 times with PBS and transferred to microfuge tubes. The cells were incubated with Annexin V (5 µl), PI (1 µl) at room temperature for 15 minutes and $1x10^4$ events were measured on the Flow cytometer device (BD Accuri C6 Plus).

3.2.9 Statistical analysis

In order to evaluate the data, statistical analysis was performed. One-way analysis of variance (ANOVA), two-way ANOVA, and Tukey's post-hoc test were conducted via GraphPad Prism software (version 9.4). P values that are below 0.05 ($p<0.05$) were considered statistically significant.

4. RESULTS AND DISCUSSION

4.1 Fluid flow rate analysis

Microfluidic systems are tools that used to perform fast, low-cost and high-throughput analysis in many different applications. Fluid flow that is controlled precisely is required in many microfluidic systems. Pumps such as piezoelectric pumps, syringe pumps, peristaltic pumps can be used to control fluid flow. On the other hand, many of these pumps are costly (Behrens et al., 2020).

Peristaltic pumps can be used to ensure recirculation flow in a closed fluid circuit. The pumps are physically isolated from sample by means of tubing, which reduces safety and contamination concerns. That's why peristaltic pumps are used in applications that require recirculating flow such as cell culture (Behrens et al., 2020; Ota et al., 2010).

As part of this thesis, it was presented a low-cost peristaltic pump which is suitable for use with microfluidic devices. The pump constructed with common tools/hardware and open-source software. The peristaltic pump represented an easy-to-use and inexpensive option to microfluidic applications.

The flow rate test was performed to express the rotational speed (rpm) of the peristaltic pump in μL/min. The fluid flow rate of the peristaltic pump was calculated depending on the rpm of the pump and diameter of the tubings. The peristaltic pump system was set up to pump distilled water through tubings into an eppendorf tube. Two different silicone tubings were used: 3.0 mm outer diameter (OD) 1.5 mm inner diameter (ID) tubing, and the other 3.8 mm OD tubing. The smaller diameter tubings were connected to both ends of the larger diameter tubing. The distilled water was pumped through the tubing at 0.1, 0.5, 1.0, 1.5, 2.0, 2.5, 3.0 rpms for one minute. The volume of fluid collected in eppendorf tube was measured with a micropipette, and the rotation speed of the pump was calculated in μl/min.

Results of this analysis indicates that the flow rate of fluid was dependent on rpm of the pump. In addition, there was a direct proportion (linear increase) between the flow rate

of the fluid and the rpm of pump. Ching et al. (2021) who developed two variants of pumps in their study agree with the idea of a linear increase between peristaltic pump speed (rpm) and flow rate. The peristaltic pump speed (rpm to µl/min) is given in figure 4.1. The detailed measurement table is in appendix 4.

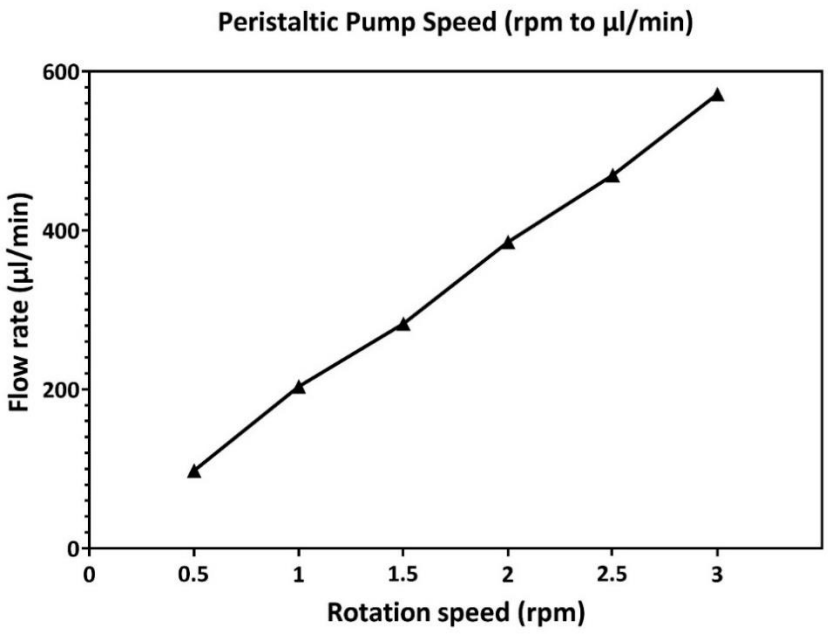

Figure 4.1 Average flow rate vs. rotation speed

4.2 Leakage analysis

A microfluidic chip with microchannel geometry in figure 3.2 was used to test the sealing of the microfluidic chip. Leakage test was performed via medium flow where the pump speed was adjusted to 0.5 rpm. The medium was passed through the microfluidic chip for 4 h. As it is explained in the study by Sözmen and Arslan Yildiz (2021) leakage test fairly relies on the material used for microfluidic chip fabrication, microchannel size and geometry. That's why microfluidic chips used in this thesis were designed by considering these parameters. As given in figure 4.2, no leakage occurred from the chip. As a result, the fabricated chip succeeded in leakage test applied in this study.

Figure 4.2 Leakage test of microfluidic chip

4.3 Occlusion analysis

The occlusion test was performed to test any possible occlusion using a microfluidic chip with microchannel geometry in figure 3.2. Medium with a volume of 1 ml and $5x10^5$ A549 cells was used to perform the occlusion test. Utilizing a peristaltic pump, the medium that contains the cells was passed through the microfluidic chip at 0.5 rpm for 2 h. The observation was carried out visually for any occlusion in the microfluidic chip. There was no occlusion in the chip. As a consequence, the fabricated chip succeeded in the test.

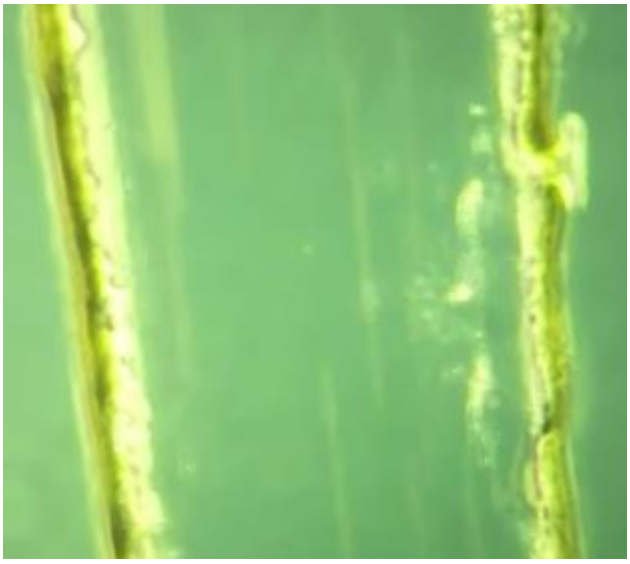

Figure 4.3 ILM image of microfluidic chip during occlusion test

4.4 LDH assay

Comparison of cell viability among control, us-GO and l-GO groups of Jurkat cells was performed by LDH assay. Jurkat cells were cultured with an expansion medium in control groups. In GO groups, cells were cultured with a mixture of expansion medium and nanomaterial (us-GO or l-GO) suspension. Also, the incorporation of flow into the system was investigated. All groups obtained during the study were examined in terms of cell viability. In addition, the toxicity of these nanomaterials was evaluated.

A 96-well plate was used in conventional cell culture. Control, us-GO, and l-GO groups were cultured in the plate. Jurkat cells were seeded at a density of $5x10^3$ cells/well in all 3 groups. The nanomaterials (us-GO or l-GO) with a concentration of 100 μg/ml were used in the GO groups.

In order to perform microfluidic cell culture, microfluidic chip designs with microchannel geometries in figure 3.2 and figure 3.3 were used. The density of nanomaterials was 100 μg/ml. The number of cells was $1x10^5$, the volume was 1 ml, and the peristaltic pump speed was 0.5 rpm for all 3 groups. The flow in the medium continued throughout the incubation.

After 24 h incubation, Jurkat cells in microfluidic cell culture were transferred to the 96-well plate, in which Jurkat cells in conventional cell culture were incubated. Then viability of the cells was assessed with LDH assay. After absorbance was measured at 490 nm and 680 nm, % of cell viability was calculated by normalizing based on the control untreated group.

In conventional cell culture, cell viability among control, us-GO, and l-GO groups was compared in figure 4.4a. According to the analysis of the assay, the cell viability of the GO-treated groups decreased compared to the control group. The cell viability of the us-GO group was lower compared to the l-GO group; however, the decreases in cell viability of both groups were not statistically significant. In other words, us-GO and l-GO did not show any significant toxicity in conventional cell culture, suggesting their good biocompatibility.

There are several studies on the toxicity of GO (Chang et al., 2011; Hu et al., 2011; Jastrzębska, Kurtycz, & Olszyna, 2012; Jia et al., 2019). In these studies, the researchers stated that the cells were sensitive to GO and also the cytotoxicity of GO changed depending on the concentration or size.

Cell viability was compared among control, us-GO, and l-GO groups in microfluidic cell culture. It is obvious in figure 4.4b that the cell viability of the GO-treated groups decreased dramatically ($p < 0.0001$compared to the control group). On the other hand, the cell viability of us-GO group showed a statistically non-significant decrease compared to the l-GO group. These results can be evaluated as follows: cells and nanomaterials interact better in the microfluidic culture medium and the cell-nanomaterial interaction was enhanced; therefore, the response of cells to these nanomaterials changed compared to a static environment.

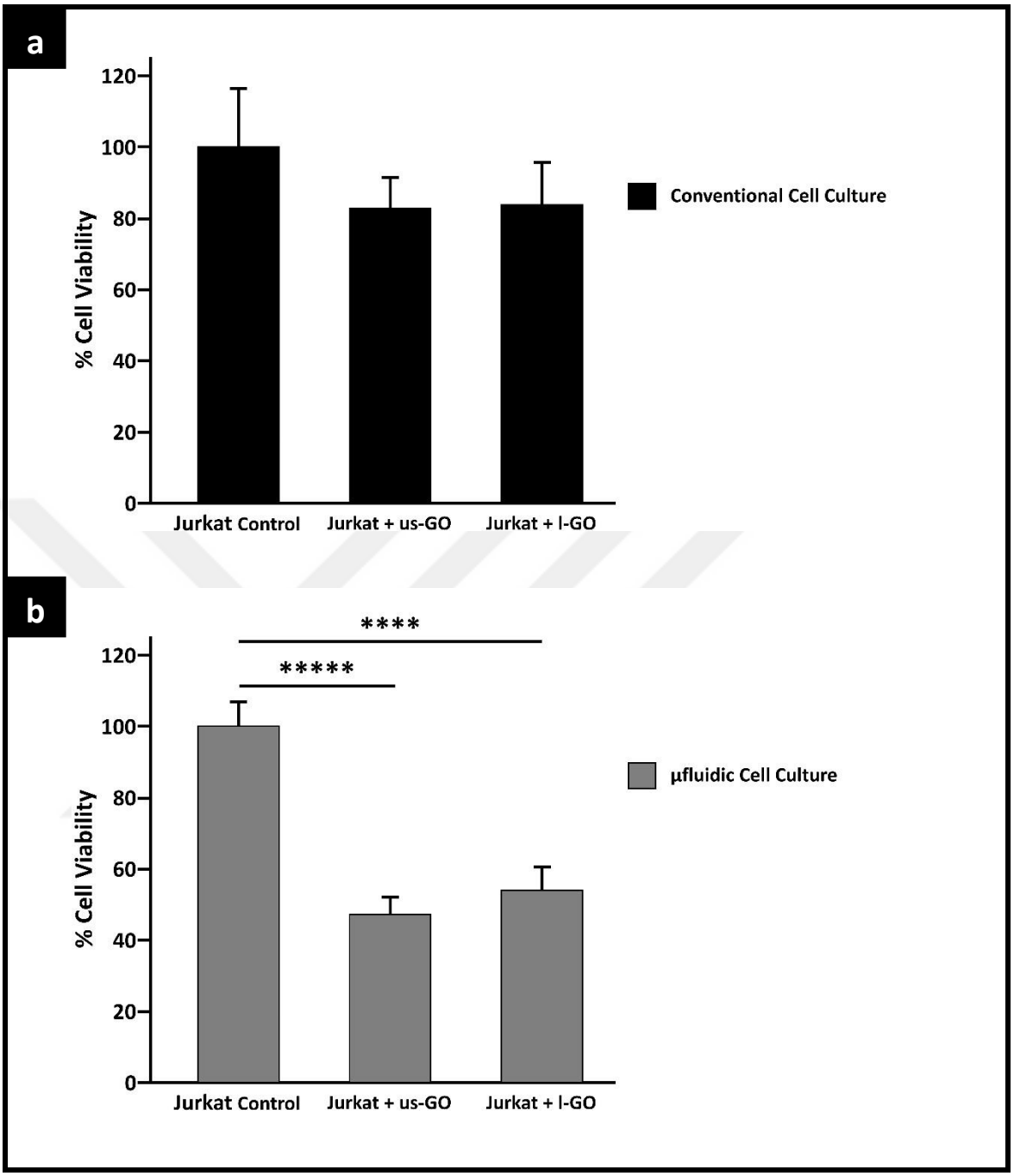

Figure 4.4 Cell vaibility of Jurkat cells. (a) Viability of the cells in conventional cell culture. (b) Viability of the cells in micrufluidic cell culture, p values: *p<0.05, **p<0.01, ***p<0.001, ****p<0.0001

Zuchowska et al. (2020) stated that GO with chemical and microbiological purity showed high biocompatibility in the microfluidic system they developed. The differences between the results obtained in our study and in that article may result from cell types used, different GO sizes, microfluidic chip design, and experimental setup (Ou et al., 2016).

Cell viability was also assessed among all the experimental groups under both static and microfluidic culture condition (Figure 4.5). In the control groups, no decrease in the cell viability of microfluidic cell culture was observed compared to conventional cell culture. Quite the contrary, an increase in cell viability of the microfluidic culture was observed, but this increase was not statistically significant. This result indicates that the microfluidic cell culture used in this study was compatible with Jurkat cells, cells were not stressed, and the viability of the cells did not decrease.

When the cells in a conventional cell culture were exposed to us-GO or l-GO, there was no significant change in cell viability. However, when the treatment was performed in a microfluidic cell culture, treatment with us-GO or l-GO significantly reduced viability of cells ($p < 0.0001$ compared to the control group in conventional cell culture). When the reduction between the us-GO group and l-GO groups was compared in microfluidic culture, this difference was not statistically significant. In addition, the difference between the us-GO group and l-GO group was not statistically significant in microfluidic cell culture.

When the cells in microfluidic culture were treated with us-GO, this treatment significantly reduced viability of cells ($p < 0.01$ compared to the conventional cell culture treated with us-GO). Similarly, when the cells in microfluidic culture were exposed with l-GO, this significantly reduced viability of cells ($p < 0.05$ compared to the conventional cell culture treated with l-GO).

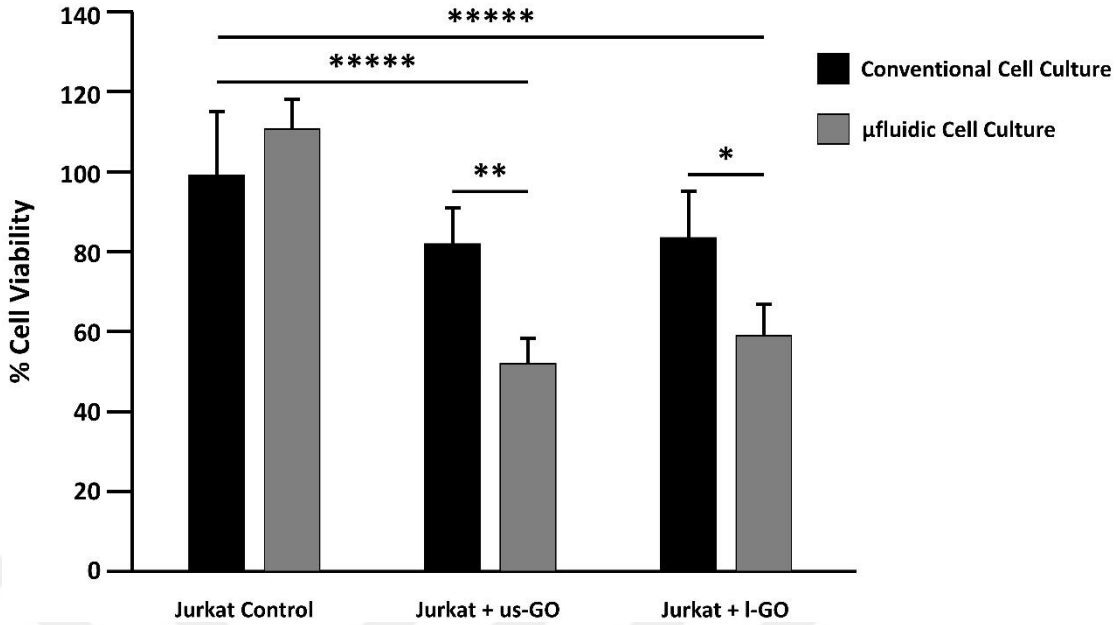

Figure 4.5 Cell viability control in conventional cell culture vs all other 5 groups, p values: *p<0.05, **p<0.01, ***p<0.001, ****p<0.0001

Jia et al. (2019) reported that the size and concentration of GO affected cell viability in conventional cell culture. In another study, Chang et al. (2011) stated that smaller sized GO induced more viability loss than larger ones at the highest concentration (200 µg/ml) in conventional cell culture.

Zamorina et al. (2021) reported that polyethylene glycol (PEG)-coated GO nanoparticles suppressed the proliferation and viability of Jurkat cells. They stated that the cytotoxic effect on these cells derived from GO in culture medium, not absorption/internalization.

In this part of the thesis, lower cell viability was observed in the smaller size GO in both conventional and microfluidic cell culture (Figure 4.4). This result can be explained because of fact that GO with smaller size could enter cells more easily than larger ones (Chang et al., 2011). Besides this cell viability of us-GO and l-GO groups in microfluidic cell culture decreased dramatically compared to conventional cell culture. This result suggested that GO could mix better in microfluidic cell culture so, cell-nanomaterial interaction increased.

4.5 Apoptosis assay

Apart from the LDH test, the effect of GO on apoptosis among control, us-GO, and l-GO groups were evaluated in a flow cytometer device using The Alexa Fluor® 488 annexin V / Dead Cell Apoptosis Kit. A 6-well plate and microfluidic chips with microchannel geometries in figure 3.2 and figure 3.3 were used to perform conventional and microfluidic cell cultures, respectively. The peristaltic pump speed was 0.5 rpm. The flow in the medium continued throughout the incubation. Nanomaterials (us-GO and l-GO) with a density of 100 μg/ml were used in GO groups. After 24 h incubation, apoptosis assay was performed following the manufacturer's instructions.

Apoptosis levels of all cell groups obtained during the thesis studies were measured so as to understand the effects of different sized GO along with different types of cell culture (Figure 4.6). The number of viable cells significantly decreased after treatment with different sized GOs in both conventional and microfluidic cell culture. Besides this it is clearly seen in figure 4.6 that while the number of necrotic cells increased significantly in us-GO and l-GO groups in conventional cell culture, the number of apoptotic cells increased significantly in us-GO and l-GO groups in microfluidic cell culture.

Kang et al. (2017) conducted research on the toxic effects of GBMs. The researchers reported that apoptosis is a response to toxicity and GO exposure provoked high levels of apoptosis depending on the material concentration.

Lim et al. (2016) examined the biological effects of four different types of GOs on vascular endothelial cells. In particular, the researchers reported that two different GOs (submicrometer and nanometer sized) caused apoptotic death through autophagy activation in endothelial cells.

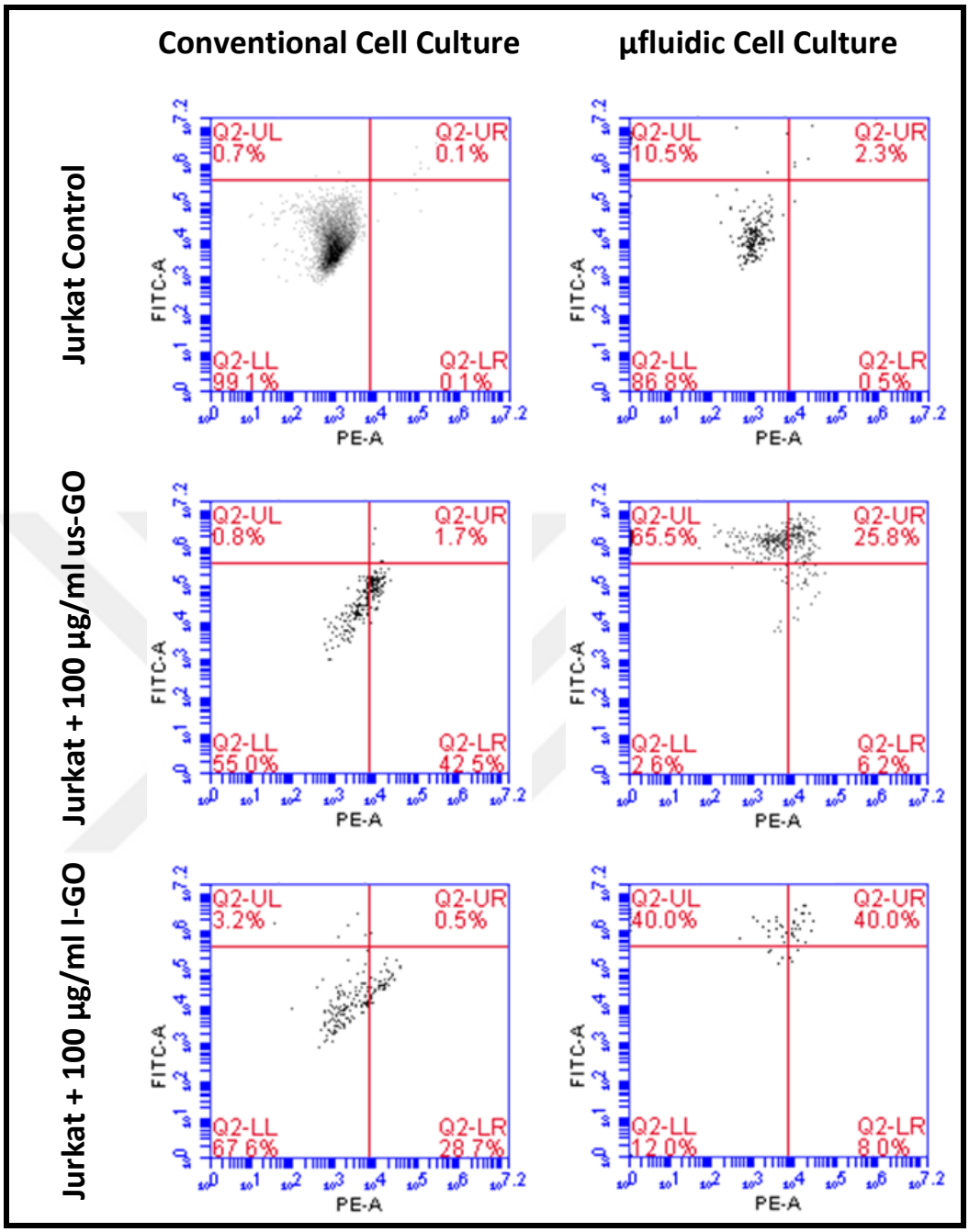

Figure 4.6 Examination of apoptotic cells. Control Jurkat cells, Jurkat cells treated with l-GO and us-GO in static and dynamic cell cultures were stained with PI. Viable cells (LL), early apoptotic cells (UL), late apoptotic and necrosis cells (UR), necrotic cells (LR) in flow cytometry analysis.

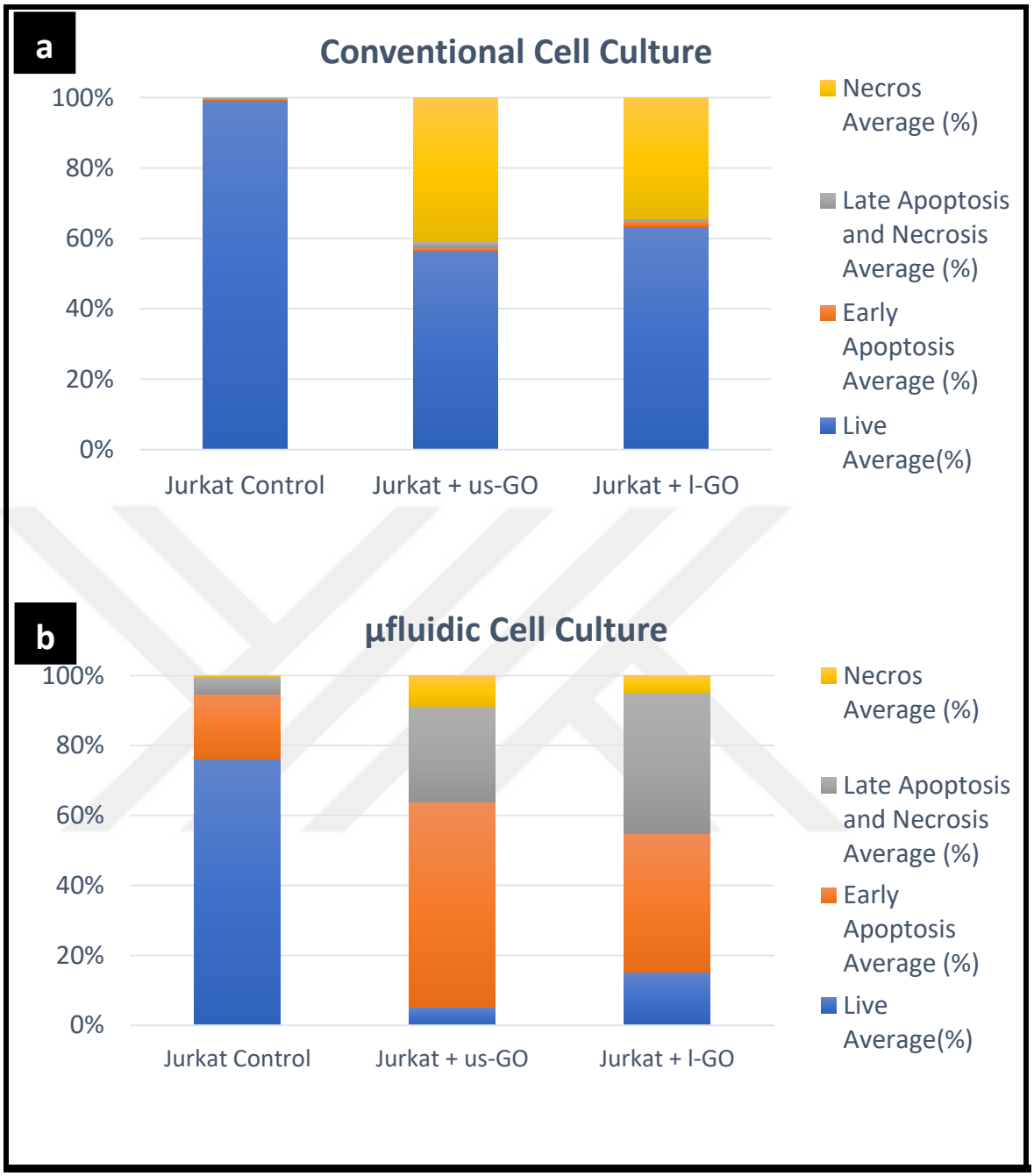

Figure 4.7 Examining results of apoptotic cells. Results of apoptosis assay after 24 h incubation of Jurkat cells treated with us-GO (100 µg/ml) and l-GO (100 µg/ml) in conventional cell culture (a) and microfluidic cell culture (b)

5. CONCLUSION

In summary, the biocompatibility of GO was investigated in this thesis. The effect of different sizes of GO on Jurkat cells was examined in both static media (conventional cell culture) and dynamic media (microfluidic cell culture). According to the results, cell viability varied in the GO groups and cell viability was dramatically reduced in microfluidic cell culture. Therefore, it is thought that the interaction of nanomaterials with cells during flow is different compared to the static media. In addition, although the size of GO affected cell viability, this was not statistically significant. In our best knowledge, this thesis is the first comparative study that was performed simultaneously in both suspension cell culture and microfluidic cell culture for analysis of GO with different sizes in view of biocompatibility. As a result, it is concluded that GO with different sizes used in this thesis indicated high toxicity and low biocompatibility in microfluidic cell culture. It is suggested that other studies can be performed by changing some parameters such as GO concentration, incubation time, fluid flow rate, microfluidic chip material, microchannel size to examine the biocompatibility of GO.

REFERENCES

Akar, Ü. (2020). Development Of a Low-Cost Microfluidic System To Detect Immunomagnetically Captured Leukemia Cells. Abdullah Gül University,Graduate School of Engineering and Sciences.

Anonymous. (2014). Pierce LDH Cytotoxicity Assay Kit, Thermo Fisher Scientific, Website: https://assets.thermofisher.com/TFS-Assets/LSG/manuals/MAN0011851_Pierce_LDH_Cytotoxicity_Asy_UG.pdf, Date of Access: 26.06.2022.

Anonymous. (2019). Annexin V-FITC Apoptosis Detection Kit, Nacalai Tesque, Website: https://www.nacalai.co.jp/global/download/pdf/AnnexinV-FITC.pdf, Date of Access: 22.06.2022.

Anonymous. (2020). Gibco Cell Culture Basics Handbook, Thermo Fisher Scientific, Website: https://assets.thermofisher.com/TFS-Assets/BID/Handbooks/gibco-cell-culture-basics-handbook.pdf, Date of Access: 07.06.2022.

Asghar, W., Yuksekkaya, M., Shafiee, H., Zhang, M., Ozen, M. O., Inci, F., . . . Demirci, U. (2016). Engineering long shelf life multi-layer biologically active surfaces on microfluidic devices for point of care applications. Scientific reports, 6(1), 1-10.

Aslım, B., & Koçancı, F. G. (2018). Üç Boyutlu Hücre Kültürü Modelleri ve Uygulamaları.

Bao, H., Pan, Y., Ping, Y., Sahoo, N. G., Wu, T., Li, L., . . . Gan, L. H. (2011). Chitosan-functionalized graphene oxide as a nanocarrier for drug and gene delivery. Small, 7(11), 1569-1578.

Behrens, M. R., Fuller, H. C., Swist, E. R., Wu, J., Islam, M., Long, Z., . . . Steward, R. (2020). Open-source, 3D-printed peristaltic pumps for small volume point-of-care liquid handling. Scientific reports, 10(1), 1-10.

Bianco, A. (2013). Graphene: safe or toxic? The two faces of the medal. Angewandte Chemie International Edition, 52(19), 4986-4997.

Bitounis, D., Ali-Boucetta, H., Hong, B. H., Min, D. H., & Kostarelos, K. (2013). Prospects and challenges of graphene in biomedical applications. Advanced Materials, 25(16), 2258-2268.

Carvalho, B. G., Ceccato, B. T., Michelon, M., Han, S. W., & de la Torre, L. G. (2022). Advanced microfluidic technologies for lipid nano-microsystems from synthesis to biological application. Pharmaceutics, 14(1), 141.

Chang, Y., Yang, S.-T., Liu, J.-H., Dong, E., Wang, Y., Cao, A., . . . Wang, H. (2011). In vitro toxicity evaluation of graphene oxide on A549 cells. Toxicology Letters, 200(3), 201-210.

Cheng, C., Li, S., Thomas, A., Kotov, N. A., & Haag, R. (2017). Functional graphene nanomaterials based architectures: biointeractions, fabrications, and emerging biological applications. Chemical reviews, 117(3), 1826-1914.

Ching, T., Vasudevan, J., Tan, H. Y., Lim, C. T., Fernandez, J., Toh, Y.-C., & Hashimoto, M. (2021). Highly-customizable 3D-printed peristaltic pump kit. HardwareX, 10, e00202.

Chung, C., Kim, Y.-K., Shin, D., Ryoo, S.-R., Hong, B. H., & Min, D.-H. (2013). Biomedical applications of graphene and graphene oxide. Accounts of chemical research, 46(10), 2211-2224.

Damiati, S., Kompella, U. B., Damiati, S. A., & Kodzius, R. (2018). Microfluidic devices for drug delivery systems and drug screening. Genes, 9(2), 103.

de Lázaro, I., Sharp, P., Gurcan, C., Ceylan, A., Stylianou, M., Kisby, T., . . . Taheri, H. (2021). Deep tissue translocation of graphene oxide sheets in human glioblastoma 3D spheroids and an orthotopic xenograft model. Advanced Therapeutics, 4(1), 2000109.

Du, D., Zou, Z., Shin, Y., Wang, J., Wu, H., Engelhard, M. H., . . . Lin, Y. (2010). Sensitive immunosensor for cancer biomarker based on dual signal amplification strategy of graphene sheets and multienzyme functionalized carbon nanospheres. Analytical chemistry, 82(7), 2989-2995.

Düven, G., Çetin, B., & Kışla, D. (2018). Çip-Üstü-Laboratuvar (ÇÜL) Teknolojisinin Gıda Mikrobiyolojisindeki Uygulamaları. Akademik Gıda, 16(1), 78-87.

Eda, G., Fanchini, G., & Chhowalla, M. (2008). Large-area ultrathin films of reduced graphene oxide as a transparent and flexible electronic material. Nature nanotechnology, 3(5), 270-274.

Erkekoğlu, P., & Baydar, T. (2021). Güncel In Vitro Sitotoksisite Testleri. Hacettepe University Journal of the Faculty of Pharmacy, 41(1), 45-63.

Fadeel, B., Bussy, C., Merino, S., Vázquez, E., Flahaut, E., Mouchet, F., . . . Vogel, U. (2018). Safety assessment of graphene-based materials: focus on human health and the environment. ACS nano, 12(11), 10582-10620.

Fotakis, G., & Timbrell, J. A. (2006). In vitro cytotoxicity assays: Comparison of LDH, neutral red, MTT and protein assay in hepatoma cell lines following exposure to cadmium chloride. Toxicology Letters, 160(2), 171-177. doi:https://doi.org/10.1016/j.toxlet.2005.07.001

Gale, B. K., Jafek, A. R., Lambert, C. J., Goenner, B. L., Moghimifam, H., Nze, U. C., & Kamarapu, S. K. (2018). A review of current methods in microfluidic device fabrication and future commercialization prospects. Inventions, 3(3), 60.

Gazzi, A., Fusco, L., Orecchioni, M., Ferrari, S., Franzoni, G., Yan, J. S., . . . Vacchi, I. A. (2020). Graphene, other carbon nanomaterials and the immune system: toward nanoimmunity-by-design. Journal of Physics: Materials, 3(3), 034009.

Güleş, Ö., & Ülker, E. (2008). Apoptozun belirlenmesinde kullanılan yöntemler. Yüzüncü Yıl Üniversitesi Veteriner Fakültesi Dergisi, 19(2), 73-78.

Gürcan, C. (2018). Grafen oksitin 2-boyutta ve 3-boyutta büyütülen kanser hücreleri üzerine etkileri. Yüksek Lisans Tezi, Ankara Üniversitesi Biyoteknoloji Enstitüsü, 82, Ankara,

Halldorsson, S., Lucumi, E., Gómez-Sjöberg, R., & Fleming, R. M. (2015). Advantages and challenges of microfluidic cell culture in polydimethylsiloxane devices. Biosensors and Bioelectronics, 63, 218-231.

Hu, W., Peng, C., Lv, M., Li, X., Zhang, Y., Chen, N., . . . Huang, Q. (2011). Protein corona-mediated mitigation of cytotoxicity of graphene oxide. ACS nano, 5(5), 3693-3700.

İçöz, K., Akar, Ü., & Ünal, E. (2020). Microfluidic Chip based direct triple antibody immunoassay for monitoring patient comparative response to leukemia treatment. Biomedical Microdevices, 22(3), 1-10.

Jastrzębska, A. M., Kurtycz, P., & Olszyna, A. R. (2012). Recent advances in graphene family materials toxicity investigations. Journal of Nanoparticle Research, 14(12), 1-21.

Jia, P.-P., Sun, T., Junaid, M., Yang, L., Ma, Y.-B., Cui, Z.-S., . . . Pei, D.-S. (2019). Nanotoxicity of different sizes of graphene (G) and graphene oxide (GO) in vitro and in vivo. Environmental Pollution, 247, 595-606.

Jiang, R. D., Shen, H., & Piao, Y.-j. (2010). The morphometrical analysis on the ultrastructure of A549 cells. Rom. J. Morphol. Embryol, 51(4), 663-667.

Jung, J. H., Cheon, D. S., Liu, F., Lee, K. B., & Seo, T. S. (2010). A graphene oxide based immuno-biosensor for pathogen detection. Angewandte Chemie, 122(33), 5844-5847.

Kang, Y., Liu, J., Wu, J., Yin, Q., Liang, H., Chen, A., & Shao, L. (2017). Graphene oxide and reduced graphene oxide induced neural pheochromocytoma-derived PC12 cell lines apoptosis and cell cycle alterations via the ERK signaling pathways. International Journal of Nanomedicine, 12, 5501.

Kapałczyńska, M., Kolenda, T., Przybyła, W., Zajączkowska, M., Teresiak, A., Filas, V., . . . Lamperska, K. (2018). 2D and 3D cell cultures–a comparison of different types of cancer cell cultures. Archives of medical science: AMS, 14(4), 910.

Karahan, Z. C. (2015), Bağışıklı Sistemi Giriş, Website: https://acikders.ankara.edu.tr/pluginfile.php/93309/mod_resource/content/0/Bağışıklık Sistemi1-Giriş.pdf, Date of Access: 14.07.2022.

Koopman, G., Reutelingsperger, C., Kuijten, G., Keehnen, R., Pals, S., & Van Oers, M. (1994). Annexin V for flow cytometric detection of phosphatidylserine expression on B cells undergoing apoptosis.

Kostarelos, K., Vincent, M., Hebert, C., & Garrido, J. A. (2017). Graphene in the design and engineering of next-generation neural interfaces. Advanced Materials, 29(42), 1700909.

Kumar, P., Nagarajan, A., & Uchil, P. D. (2018). Analysis of Cell Viability by the Lactate Dehydrogenase Assay. Cold Spring Harb Protoc, 2018(6). doi:10.1101/pdb.prot095497

Lee, K., Kim, S.-E., Doh, J., Kim, K., & Chung, W. K. (2021). User-friendly image-activated microfluidic cell sorting technique using an optimized, fast deep learning algorithm. Lab on a Chip, 21(9), 1798-1810.

Lim, M.-H., Jeung, I. C., Jeong, J., Yoon, S.-J., Lee, S.-H., Park, J., . . . Min, J.-K. (2016). Graphene oxide induces apoptotic cell death in endothelial cells by activating autophagy via calcium-dependent phosphorylation of c-Jun N-terminal kinases. Acta biomaterialia, 46, 191-203. doi:https://doi.org/10.1016/j.actbio.2016.09.018

Mark, D., Haeberle, S., Roth, G., Stetten, F. v., & Zengerle, R. (2010). Microfluidic lab-on-a-chip platforms: requirements, characteristics and applications. Microfluidics based microsystems, 305-376.

McDonald, J. C., Duffy, D. C., Anderson, J. R., Chiu, D. T., Wu, H., Schueller, O. J., & Whitesides, G. M. (2000). Fabrication of microfluidic systems in poly (dimethylsiloxane). ELECTROPHORESIS: An International Journal, 21(1), 27-40.

Mehling, M., & Tay, S. (2014). Microfluidic cell culture. Current opinion in Biotechnology, 25, 95-102.

Menaa, F., Abdelghani, A., & Menaa, B. (2015). Graphene nanomaterials as biocompatible and conductive scaffolds for stem cells: impact for tissue engineering and regenerative medicine. Journal of tissue engineering and regenerative medicine, 9(12), 1321-1338.

Metto, E. C., Evans, K., Barney, P., Culbertson, A. H., Gunasekara, D. B., Caruso, G., . . . Culbertson, C. T. (2013). An integrated microfluidic device for monitoring changes in nitric oxide production in single t-lymphocyte (jurkat) cells. Analytical chemistry, 85(21), 10188-10195.

Montano, M. (2014). Translational biology in medicine: Elsevier.

Morsink, M. A., Willemen, N. G., Leijten, J., Bansal, R., & Shin, S. R. (2020). Immune organs and immune cells on a chip: an overview of biomedical applications. Micromachines, 11(9), 849.

Mou, L., & Jiang, X. (2017). Materials for microfluidic immunoassays: a review. Advanced healthcare materials, 6(15), 1601403.

Mukherjee, S. P., Bottini, M., & Fadeel, B. (2017). Graphene and the immune system: a romance of many dimensions. Frontiers in immunology, 8, 673.

Naher, S., Orpen, D., Brabazon, D., Poulsen, C. R., & Morshed, M. M. (2011). Effect of micro-channel geometry on fluid flow and mixing. Simulation Modelling Practice and Theory, 19(4), 1088-1095. doi:https://doi.org/10.1016/j.simpat.2010.12.008

Nguyen, N.-T., Wereley, S. T., & Shaegh, S. A. M. (2019). Fundamentals and applications of microfluidics: Artech house.

Niculescu, A.-G., Chircov, C., Bîrcă, A. C., & Grumezescu, A. M. (2021). Fabrication and applications of microfluidic devices: A review. International Journal of Molecular Sciences, 22(4), 2011.

Orecchioni, M., Jasim, D. A., Pescatori, M., Manetti, R., Fozza, C., Sgarrella, F., . . . Delogu, L. G. (2016). Molecular and genomic impact of large and small lateral dimension graphene oxide sheets on human immune cells from healthy donors. Advanced healthcare materials, 5(2), 276-287.

Orecchioni, M., Ménard-Moyon, C., Delogu, L. G., & Bianco, A. (2016). Graphene and the immune system: challenges and potentiality. Advanced drug delivery reviews, 105, 163-175.

Orecchioni, M., Bedognetti, D., Sgarrella, F., Marincola, F. M., Bianco, A., & Delogu, L. G. (2014). Impact of carbon nanotubes and graphene on immune cells. Journal of translational medicine, 12(1), 1-11

Ota, H., Yamamoto, R., Deguchi, K., Tanaka, Y., Kazoe, Y., Sato, Y., & Miki, N. (2010). Three-dimensional spheroid-forming lab-on-a-chip using micro-rotational flow. Sensors and Actuators B: Chemical, 147(1), 359-365.

Ou, L., Song, B., Liang, H., Liu, J., Feng, X., Deng, B., . . . Shao, L. (2016). Toxicity of graphene-family nanoparticles: a general review of the origins and mechanisms. Particle and fibre toxicology, 13(1), 1-24.

Özbey, A. (2011). PDMS tabanlı mikroakışkan platformları oluşturmak ve karakterize etmek. Yüksek Lisans Tezi, İstanbul Teknik Üniversitesi, Fen Bilimleri Enstitüsü, Makine Mühendisliği Anabilim Dalı, 101, İstanbul.

Pattanayak, P., Singh, S. K., Gulati, M., Vishwas, S., Kapoor, B., Chellappan, D. K., . . . Gupta, P. K. (2021). Microfluidic chips: recent advances, critical strategies in design, applications and future perspectives. Microfluidics and Nanofluidics, 25(12), 1-28.

Russier, J., Treossi, E., Scarsi, A., Perrozzi, F., Dumortier, H., Ottaviano, L., . . . Bianco, A. (2013). Evidencing the mask effect of graphene oxide: a comparative study on primary human and murine phagocytic cells. Nanoscale, 5(22), 11234-11247.

Qu, Y., He, F., Yu, C., Liang, X., Liang, D., Ma, L., . . . Wu, J. (2018). Advances on graphene-based nanomaterials for biomedical applications. Materials Science and Engineering: C, 90, 764-780.

Ren, K., Zhou, J., & Wu, H. (2013). Materials for microfluidic chip fabrication. Accounts of chemical research, 46(11), 2396-2406.

Rizzo, D. J., Veber, G., Cao, T., Bronner, C., Chen, T., Zhao, F., . . . Fischer, F. R. (2018). Topological band engineering of graphene nanoribbons. Nature, 560(7717), 204-208.

Rodrigues, A. F., Newman, L., Lozano, N., Mukherjee, S. P., Fadeel, B., Bussy, C., & Kostarelos, K. (2018). A blueprint for the synthesis and characterisation of thin graphene oxide with controlled lateral dimensions for biomedicine. 2D Materials, 5(3), 035020.

Sattari, A., Hanafizadeh, P., & Hoorfar, M. (2020). Multiphase flow in microfluidics: From droplets and bubbles to the encapsulated structures. Advances in Colloid and Interface Science, 282, 102208.

Saydé, T., El Hamoui, O., Alies, B., Gaudin, K., Lespes, G., & Battu, S. (2021). Biomaterials for three-dimensional cell culture: From applications in oncology to nanotechnology. Nanomaterials, 11(2), 481.

Sgonc, R., & Gruber, J. (1998). Apoptosis detection: an overview. Experimental gerontology, 33(6), 525-533.

Shen, H., Zhang, L., Liu, M., & Zhang, Z. (2012). Biomedical applications of graphene. Theranostics, 2(3), 283.

Sözmen, A. B., & Arslan Yildiz, A. (2021). Cost-effective and rapid prototyping of PMMA microfluidic device via polymer-assisted bonding. Microfluidics and Nanofluidics, 25(8), 1-11.

Sun, X., Liu, Z., Welsher, K., Robinson, J. T., Goodwin, A., Zaric, S., & Dai, H. (2008). Nano-graphene oxide for cellular imaging and drug delivery. Nano research, 1(3), 203-212.

Szunerits, S., & Boukherroub, R. (2016). Antibacterial activity of graphene-based materials. Journal of Materials Chemistry B, 4(43), 6892-6912.

Thurnherr, T., Su, D. S., Diener, L., Weinberg, G., Manser, P., Pfänder, N., . . . Krug, H. F. (2009). Comprehensive evaluation of in vitro toxicity of three large-scale produced carbon nanotubes on human Jurkat T cells and a comparison to crocidolite asbestos. Nanotoxicology, 3(4), 319-338

Vashishtha, S., Nazarali, A., & Dimmock, J. (1998). Application of fluorescence microscopy to measure apoptosis in Jurkat T cells after treatment with a new investigational anticancer agent (NC 1213). Cellular and molecular neurobiology, 18(4), 437-445.

Wang, K., Ruan, J., Song, H., Zhang, J., Wo, Y., Guo, S., & Cui, D. (2011). Biocompatibility of graphene oxide. Nanoscale Res Lett, 6(1), 1-8.

Wang, Z., Samanipour, R., Koo, K., & Kim, K. (2015). Organ-on-a-chip platforms for drug delivery and cell characterization: A review. Sens. Mater, 27(6), 487-506.

Whitesides, G. M. (2006). The origins and the future of microfluidics. Nature, 442(7101), 368-373.

Wu, M.-H., Huang, S.-B., & Lee, G.-B. (2010). Microfluidic cell culture systems for drug research. Lab on a Chip, 10(8), 939-956.

Yang, Y., Asiri, A. M., Tang, Z., Du, D., & Lin, Y. (2013). Graphene based materials for biomedical applications. Materials today, 16(10), 365-373.

Young, E. W., & Beebe, D. J. (2010). Fundamentals of microfluidic cell culture in controlled microenvironments. Chemical Society Reviews, 39(3), 1036-1048.

Zamorina, S., Khramtsov, P., Rayev, M., Timganova, V., Bochkova, M., Nechaev, A., . . . Litvinova, L. (2021). Graphene Oxide Nanoparticels Interaction with Jurkat Cell Line in Cell-IQ System. Paper presented at the Doklady Biochemistry and Biophysics.

Zhang, Q., Wu, Z., Li, N., Pu, Y., Wang, B., Zhang, T., & Tao, J. (2017). Advanced review of graphene-based nanomaterials in drug delivery systems: Synthesis, modification, toxicity and application. Materials Science and Engineering: C, 77, 1363-1375.

Zhi, X., Fang, H., Bao, C., Shen, G., Zhang, J., Wang, K., . . . Cui, D. (2013). The immunotoxicity of graphene oxides and the effect of PVP-coating. Biomaterials, 34(21), 5254-5261.

Zuchowska, A., Buta, A., Dabrowski, B., Jastrzebska, E., Zukowski, K., & Brzozka, Z. (2020). 3D and 2D cell models in a novel microfluidic tool for evaluation of highly chemically and microbiologically pure graphene oxide (GO) as an effective drug carrier. Sensors and Actuators B: Chemical, 302, 127064.

APPENDICES

APPENDIX 1

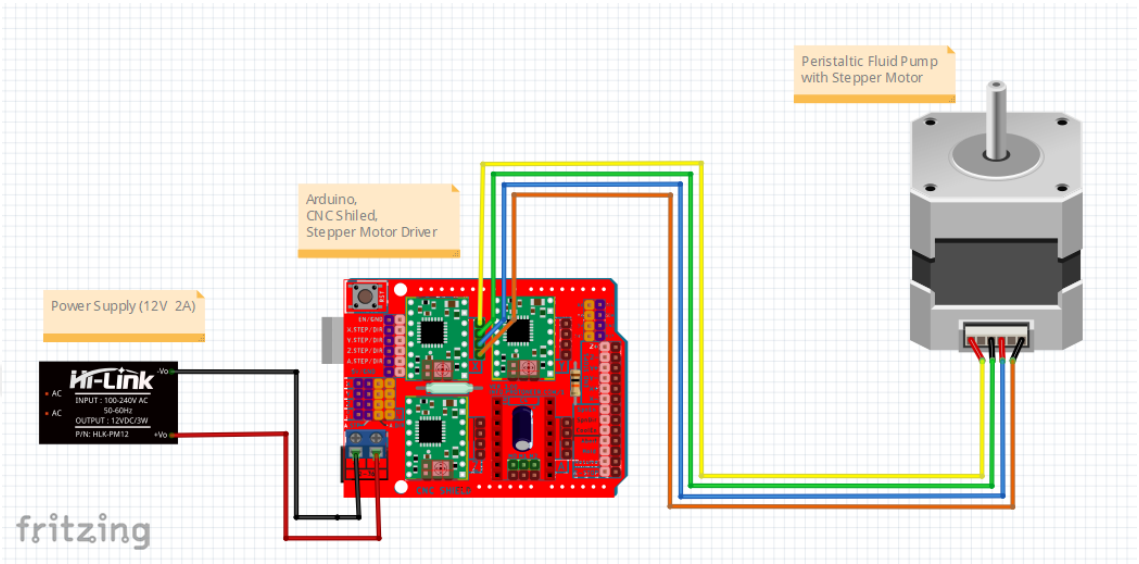

Peristaltic pump system wiring diagram

APPENDIX 2

```
#include <AccelStepper.h>
#define MotorEnb 8
AccelStepper stepper(1,2,5);
String inputString = "";
boolean stringComplete = false;
int cmdIndex;
String cmdString = "";
float SpeedValue = 2;  //rpm!
boolean modeValue = false;
void setup() {
  pinMode(MotorEnb,OUTPUT);
  digitalWrite(MotorEnb,!modeValue);
  stepper.setMaxSpeed(5000);
  stepper.setSpeed(SpeedValue*200*16/60);
  Serial.begin(9600);
  inputString.reserve(40);
  cmdString.reserve(20);
}
void loop() {
  while (Serial.available())
  {
    char inChar = (char)Serial.read();
    if (inChar == '\n')
    {
      stringComplete = true;
    }
```

Arduino Programming (in Arduino IDE)

```
  else
  {
    inputString += inChar;
  }
 }

 if (stringComplete)
 {
  cmdIndex = inputString.indexOf(' ');
  cmdString = inputString.substring(0,cmdIndex);
  if (cmdString == "spd")
  {
    SpeedValue = (inputString.substring(cmdIndex+1)).toFloat();
    if(SpeedValue>=0.01 & SpeedValue<=50)
    {
     stepper.setSpeed(SpeedValue*200*16/60);
    }
  }
  else if (cmdString == "ssc")
  {
    modeValue = (boolean) (inputString.substring(cmdIndex+1)).toInt();
    digitalWrite(MotorEnb,!modeValue);
  }
  inputString = "";
  stringComplete = false;
 }
  stepper.runSpeed();
}
```

Arduino Programming (in Arduino IDE) (continued)

APPENDIX 3

```
using System;
using System.Collections.Generic;
using System.ComponentModel;
using System.Data;
using System.Drawing;
using System.Linq;
using System.Text;
using System.Threading.Tasks;
using System.Windows.Forms;
using System.IO.Ports;
namespace Peristaltic_Pump_Application
{
   public partial class Form1 : Form
   {
      String[] portList;
      bool connectionStatus = false;
      string speed;
      int hour = 0, minute = 0, second = 0;
      public Form1()
      {
         InitializeComponent();
      }
      void showPort()
      {
         comboBox1.Items.Clear();
         portList = SerialPort.GetPortNames();
         foreach (string portName in portList)
```

Source Code of Peristaltic Pump Application

```
    {
        comboBox1.Items.Add(portName);
        if (portList[0] != null)
        {
            comboBox1.SelectedItem = portList[0];
        }
    }
}

private void Form1_Load(object sender, EventArgs e)
{
    groupBox2.Enabled = false;
    groupBox3.Enabled = false;
    groupBox4.Enabled = false;
    button4.Enabled = false;
    timer1.Interval = 1000;
    textBox1.Text = "2";
    showPort();
}

private void button2_Click(object sender, EventArgs e)
{
    showPort();
}

private void button1_Click(object sender, EventArgs e)
{
    if (connectionStatus == false)
```

Source Code of Peristaltic Pump Application (continued)

```
    {
        serialPort1.PortName = comboBox1.GetItemText(comboBox1.SelectedItem);
        serialPort1.BaudRate = 9600;
        serialPort1.Open();
        comboBox1.Enabled = false;
        label2.Text = "Connected";
        button2.Enabled = false;
        connectionStatus = true;
        button1.Text = "Disconnect";
        groupBox2.Enabled = true;
    }
    else
    {
        //serialPort1.Write("ssc 0\n");
        serialPort1.Close();
        connectionStatus = false;
        button1.Text = "Connect";
        comboBox1.Enabled = true;
        label2.Text = "Not Connected";
        //label8.Text = "Off";
        button2.Enabled = true;
        groupBox2.Enabled = false;
        groupBox3.Enabled = false;
        groupBox4.Enabled = false;
    }
}

private void button3_Click(object sender, EventArgs e)
```

Source Code of Peristaltic Pump Application (continued)

```
        {
            serialPort1.Write("ssc 1\n");
            timer1.Start();
            label8.Text = "On";
            button3.Enabled = false;
            button4.Enabled = true;
            groupBox4.Enabled = true;
        }
/* Some deviation happens in the value on the stopwatch
        private void timer1_Tick(object sender, EventArgs e)
        {
            second++;
            if (second >= 60)
            {
                minute++;
                second = 0;
                if (minute >= 60)
                {
                    hour++;
                    minute = 0;
                }
            }
            label.Text = String.Format("{ 0:D2}", hour);
            label.Text = String.Format("{0:D2}", minute);
            label.Text = String.Format("{0:D2}", second);
*/
private void button6_Click(object sender, EventArgs e)
        {
```

Source Code of Peristaltic Pump Application (continued)

```
    if (serialPort1.IsOpen) serialPort1.Close();
    this.Close();
}

private void button4_Click(object sender, EventArgs e)
{
    serialPort1.Write("ssc 0\n");
    timer1.Stop();
    hour = 0;
    minute = 0;
    second = 0;
    label8.Text = "Off";
    button3.Enabled = true;
    button4.Enabled = false;
}
```

Source Code of Peristaltic Pump Application (continued)

APPENDIX 4

Peristaltic pump speed in detail (rpm to µl/min)

rpm	µl/min	µl/min	µl/min	Average (µl)	Standard Deviation
0.1	14.2	15.1	16.9	15.4	1.37
0.5	98.2	95.2	100.4	97.93	2.61
1	199	205	207	203.67	4.16
1.5	287	282	279	282.67	4.04
2	384	384	388	385.33	2.31
2.5	467	472	469	469.33	2.52
3	572	572	570	571.33	1.15

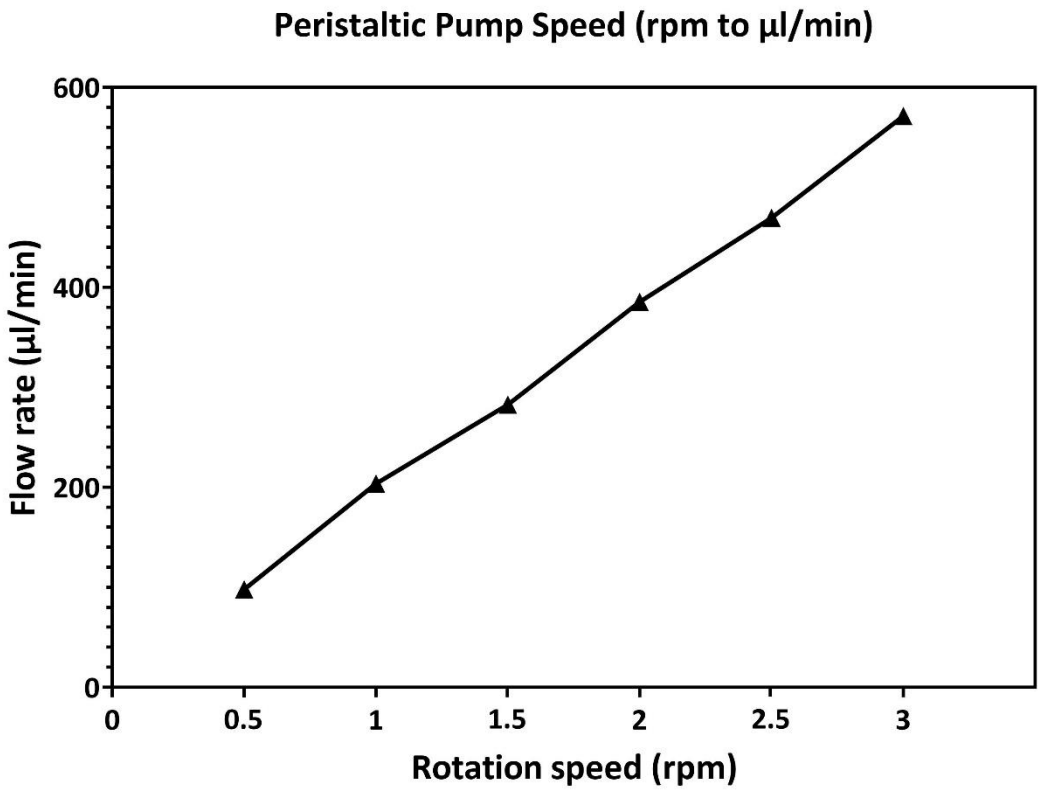

Peristaltic Pump Speed (rpm to µl/min)